IWMI
Working
Paper

187

From the Mountains to the Plains:
Impact of Climate Change on Water Resources in the Koshi River Basin

Luna Bharati, Utsav Bhattarai, Ambika Khadka, Pabitra Gurung, Luis E. Neumann, David J. Penton, Sanita Dhaubanjar and Santosh Nepal

IWMI International Water Management Institute

ICIMOD

CSIRO

CGIAR RESEARCH PROGRAM ON Water, Land and Ecosystems

Working Papers

The publications in this series record the work and thinking of IWMI researchers, and knowledge that the Institute's scientific management feels is worthy of documenting. This series will ensure that scientific data and other information gathered or prepared as a part of the research work of the Institute are recorded and referenced. Working Papers could include project reports, case studies, conference or workshop proceedings, discussion papers or reports on progress of research, country-specific research reports, monographs, etc. Working Papers may be copublished, by IWMI and partner organizations.

Although most of the reports are published by IWMI staff and their collaborators, we welcome contributions from others. Each report is reviewed internally by IWMI staff. The reports are published and distributed both in hard copy and electronically (www.iwmi.org) and where possible all data and analyses will be available as separate downloadable files. Reports may be copied freely and cited with due acknowledgment.

About IWMI

IWMI's mission is *to provide evidence-based solutions to sustainably manage water and land resources for food security, people's livelihoods and the environment.* IWMI works in partnership with governments, civil society and the private sector to develop scalable agricultural water management solutions that have a tangible impact on poverty reduction, food security and ecosystem health.

IWMI Working Paper 187

From the Mountains to the Plains: Impact of Climate Change on Water Resources in the Koshi River Basin

Luna Bharati, Utsav Bhattarai, Ambika Khadka, Pabitra Gurung, Luis E. Neumann, David J. Penton, Sanita Dhaubanjar and Santosh Nepal

International Water Management Institute

The authors: Luna Bharati is Principal Researcher – Hydrology and Water Resources at the International Water Management Institute (IWMI), based at the Center for Development Research (ZEF) in Bonn, Germany; Utsav Bhattarai was a consultant, and Ambika Khadka and Pabitra Gurung were Research Officers at IWMI, Lalitpur, Nepal, at the time this research study was conducted; Luis E. Neumann and David J. Penton were both at Land and Water, Commonwealth Scientific and Industrial Research Organisation (CSIRO), Australia, at the time this research study was conducted; Sanita Dhaubanjar is a Research Officer at IWMI, Lalitpur, Nepal; and Santosh Nepal is a Water and Climate Specialist at the International Centre for Integrated Mountain Development (ICIMOD), Kathmandu, Nepal.

Bharati, L.; Bhattarai, U.; Khadka, A.; Gurung, P.; Neumann, L. E.; Penton, D. J.; Dhaubanjar, S.; Nepal, S. 2019. *From the mountains to the plains: impact of climate change on water resources in the Koshi River Basin*. Colombo, Sri Lanka: International Water Management Institute (IWMI). 49p. (IWMI Working Paper 187). doi: 10.5337/2019.205

/ climate change / climatic data / water resources / water balance / water yield / water availability / mountains / plains / river basin management / soil analysis / soil water balance / calibration / spatial distribution / hydropower / precipitation / evapotranspiration / temperature / rainfall / monsoon climate / catchment areas / hydrological data / impact assessment / models / flow discharge / runoff / land use / seasonal variation / China / Nepal / India /

ISSN 2012-5763
e-ISSN 2478-1134
ISBN 978-92-9090-885-2

Please direct inquiries and comments to: *IWMI-Publications@cgiar.org*

A free copy of this publication can be downloaded at www.iwmi.org/publications/iwmi-working-papers

Acknowledgements

This paper was prepared by the International Water Management Institute (IWMI) under the Koshi Basin Programme led by the International Centre for Integrated Mountain Development (ICIMOD), which was supported by the Australian government through the Sustainable Development Investment Portfolio for South Asia. The authors are grateful to Dr. Alan Nicol (Strategic Program Leader – Promoting Sustainable Growth, IWMI) and Dr. Matthew McCartney (Research Group Leader – Water Futures, Growth and Natural Capital, IWMI) for reviewing various versions of this paper; and special thanks go to Mahen Chandrasoma (Senior Production Editor, IWMI) for doing the final language edits on the paper.

Collaborators

International Water Management Institute (IWMI)

International Centre for Integrated Mountain Development (ICIMOD), Kathmandu, Nepal

Land and Water, Commonwealth Scientific and Industrial Research Organisation (CSIRO), Australia

Donors

International Centre for Integrated Mountain Development (ICIMOD), Kathmandu, Nepal

Land and Water, Commonwealth Scientific and Industrial Research Organisation (CSIRO), Australia

This research was carried out as part of the CGIAR Research Program on Water, Land and Ecosystems (WLE) and supported by Funders contributing to the CGIAR Trust Fund (https://www.cgiar.org/funders/).

Contents

Acronyms and Abbreviations

AR	Assessment Report
ASCII	American Standard Code for Information Interchange
CC	Climate Change
CFSR	Climate Forecast System Reanalysis
CO_2	Carbon dioxide
DEM	Digital Elevation Model
DHM	Department of Hydrology and Meteorology
DREAM	DiffeRential Evolution Adaptive Metropolis
ET	Evapotranspiration
FDC	Flow Duration Curve
GCM	General Circulation Model
GIS	Geographic information system
H	Hills
HKH	Hindu Kush Himalaya
HRU	Hydrologic Response Units
Hydrosheds	Hydrological data and maps based on SHuttle Elevation Derivatives at multiple Scales
ICIMOD	International Centre for Integrated Mountain Development
IGP	Indo-Gangetic Plains
IHA	Indicators of Hydrologic Alteration
IMD	India Meteorological Department
IPCC	Intergovernmental Panel on Climate Change
ISRIC	World Soil Information (legally registered as the International Soil Reference and Information Centre)
IWR	Irrigation Water Requirement
JICA	Japan International Cooperation Agency
LATTIME	Lateral Flow Travel Time
LULC	Land Use/Land Cover
M	Mountain
NSE	Nash-Sutcliffe Efficiency
PBIAS	Percent Bias
RCP	Representative Concentration Pathways
RMSE	Root mean square error
RSR	Ratio of the root mean square deviation to the standard deviation
SD	Standard Deviation
SFTMP	Snowfall Temperature
SOTER	Soil and Terrain database system (from ISRIC)
SMTMP	Snowmelt Base Temperature
SRTM	Shuttle Radar Topography Mission
SWAT	Soil and Water Assessment Tool
TM	Transmountain
TRMM	Tropical Rainfall Measuring Mission

Summary

The Koshi Basin, spread across China, Nepal and India, is perceived as having high potential for hydropower and irrigation development, both seen as ways to promote economic development in the region. As climate change (CC) is likely to impact future water resources, it is very important to consider CC in future planning. This paper quantifies and assesses the past and projected future spatial and temporal water balances in the Koshi Basin. A Soil and Water Assessment Tool (SWAT) model was set up, calibrated and validated using measured daily flow data from the basin from 1999 to 2006. The CC analysis is based on the most recent Intergovernmental Panel on Climate Change (IPCC) Fifth Assessment Report (AR5) "Representative Concentration Pathways" (RCPs 4.5 and 8.5). The delta change approach was used to generate daily future time series climate data for 2021-2050, considering historical data from 1998-2008 as reference.

Results show that the annual average precipitation, actual evapotranspiration (ET) and net water yield for the reference period are 1,720 mm, 520 mm and 1,124 mm, respectively, with over 75% of precipitation and flow occurring during the monsoon season. The precipitation and net water yield are lowest in the transmountain region and the Tibetan plateau. The values are highest in the mountain region, followed by the hills and Indo-Gangetic Plains. Approximately 65% of average annual precipitation is converted to flows, indicating high water availability. Actual ET, which indicates water use by plants, is highest in the Indo-Gangetic Plains region due to the presence of irrigated agriculture and a few forested mountain watersheds. There is, therefore, a clear mismatch between the area where water availability is highest (mountains) and where water use is highest (Indo-Gangetic Plains). As most of the water from the mountain and hill regions eventually flows down to the plains, the mountain and hill regions in Nepal are important for maintaining agriculture in the plains in both Nepal and India.

Flow analyses show that high-flow pulses (exceeding 75% of daily flows) occur two to five times annually and last for 2 to 20 days during the monsoon season. Extreme low flows occur two to nine times annually and last up to 25 days during the dry season. These results indicate the high temporal variability of flows in the basin. The information on these extreme weather events could be very useful in water-induced disaster management in this region, and also for planning long-term hydraulic structures. The frequent occurrences of both high- and low-flow events demonstrate the existing vulnerability of the region to both floods and droughts, leading to a very risk-prone livelihood system.

The CC projections show an increasing trend in precipitation and net water yield for most of the basin, except the transmountain region. Actual ET also shows an increasing trend for both CC pathways (RCPs 4.5 and 8.5) throughout the basin. Comparison of flow ranges between the past and projected data indicates that future changes during the dry season are within the past data ranges. However, the future monsoon flows will be higher than the past as demonstrated by higher averages as well as maximum flows. An increasing trend is seen in the high-flow pulse frequency, and occurrences of high flows are shifting towards the latter part of the monsoon. Therefore, flooding occurrences in the monsoon are expected to increase with CC.

Results also show that the seasonal variation in contribution to annual flow volume at the outlet of the Koshi Basin for the reference and future periods remained very similar, with over 75% of the total annual flow occurring within the monsoon season. Therefore, the monsoon will remain the main hydrological driver, variability will continue to be high, future dry seasons will be similar to the past dry seasons, and future monsoons will likely be stronger and wetter with increased flood risk.

INTRODUCTION

There is a growing focus among the scientific community on understanding the Himalayan river basins with several recent studies investigating the biophysical processes (e.g., Lutz et al. 2014; Immerzeel et al. 2013; Devkota and Gyawali 2015; Nepal 2016). The Himalayan river basins are still considered to be data and information scarce, relative to other regions; scientific studies, especially related to the physical system, are limited. This is primarily due to unavailability and sometimes inaccessibility of long-term hydrological and climate data of good quality and coverage, as well as lack of rigorous analysis of the existing accessible information. The complex topography and extreme climate also make it difficult for climate scientists to construct hydrological and climatic sequences with good spatial and temporal coverage. Nonetheless, decision makers need to explore possible future development scenarios.

The Koshi River Basin is perceived as having high potential for hydropower and irrigation development, both seen as ways to promote economic development in the region. The respective governments (i.e., China, Nepal and India) are interested in building water infrastructure to develop energy production and water supply. There have been a few enabling steps in this direction, such as the recently signed power trade agreement between Nepal and India. So far, a basin development strategy, which goes beyond national and sectorial plans, does not exist. Future water infrastructure is being designed primarily at individual project level without real consideration of the impacts/ benefits outside of the project objectives, such as downstream impacts, environmental flows, impact on local livelihoods, etc. A prerequisite for developing any future basin plans is to carry out water resource assessments, which quantify both spatial and temporal water availability in the basin. Furthermore, as climate change (CC) is likely to impact future water resources, it is very important to consider CC in future planning.

The main objective of this study was to assess the spatial and temporal water balances in the Koshi Basin in China, Nepal and India, and quantify the impact of CC on the basin. The Soil and Water Assessment Tool (SWAT) model was used to carry out the analysis at sub-basin level. The study is a follow-up to previous studies in the Koshi Basin by the authors (Bharati et al. 2014, 2016). In the previous studies, the Koshi Basin was limited to the mountain and hill regions in China and Nepal. However, in this new, updated study, the outlet of the basin is where the Koshi River joins the main branch of the Ganges (Figure 1) in India. This larger basin includes the transmountain, mountain and hills as well as the Indo-Gangetic Plains (IGP). The transmountain region is behind the Himalayan mountain range in the main Tibetan Plateau. The current study incorporated better input data for the model, including: (i) data from high-altitude stations in the mountains, which were previously not available; (ii) remotely sensed datasets such as Tropical Rainfall Measuring Mission (TRMM); (iii) more detailed land cover and soil maps (see section *Methods and Data*); and (iv) CC analysis was based on the most recent Intergovernmental Panel on Climate Change (IPCC) Fifth Assessment Report (AR5) (IPCC 2014). The current study also compared the performance of the more detailed SWAT model to a simple conceptual model GR4J to assess the impact of model structure on model performance (see section *Results and Discussion*). Furthermore, the Indicators of Hydrologic Alteration (IHA) version 7.1 was used to analyze extreme weather events.

STUDY AREA

The Koshi River is one of the largest tributaries of the Ganges River. The catchment area of the Koshi River up to its confluence with the Ganges River is 87,311 km^2, of which 28,300 km^2 lies in China, 39,407 km^2 in Nepal and 19,604 km^2 in India.

FIGURE 1. Map of the Koshi River Basin showing the administrative boundaries and the four ecological regions.

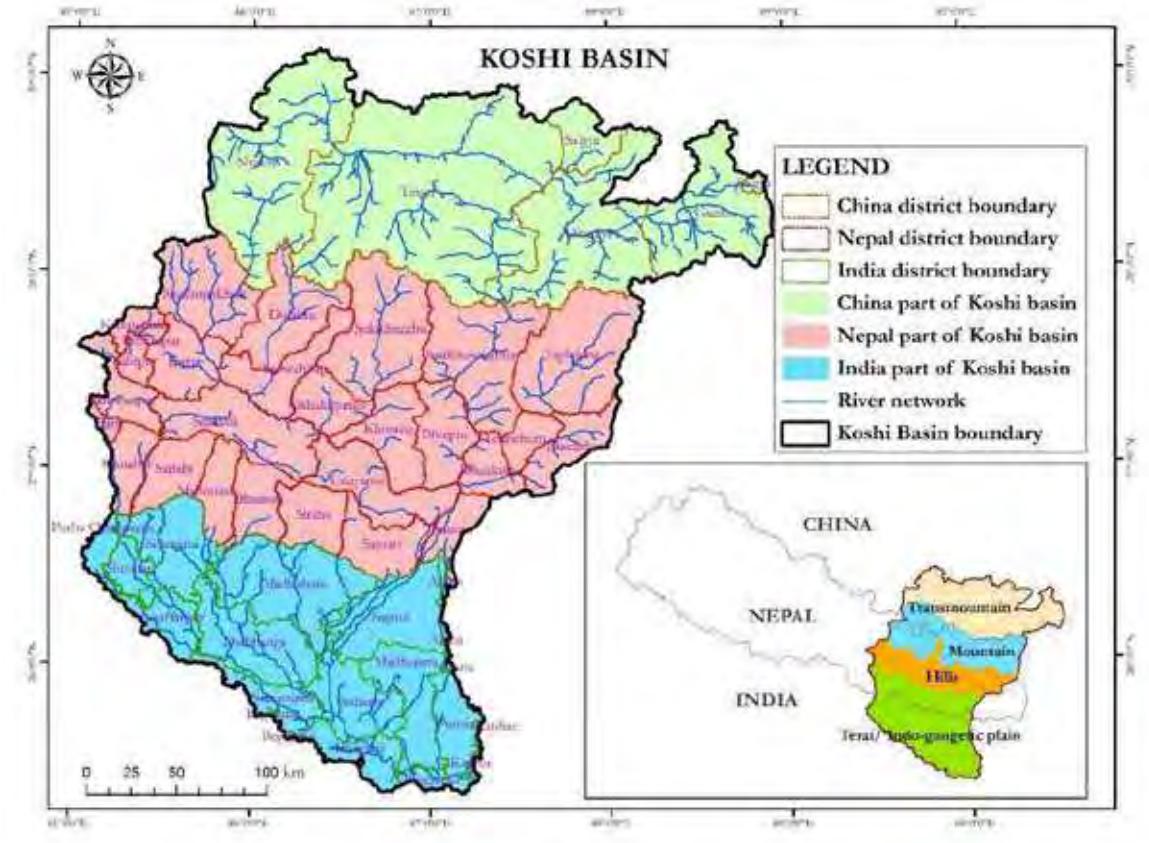

The basin covers five districts in China, 27 districts in Nepal and 16 districts in India. The basin area lies within latitudes 26°54’47’’ N to 25°24’43’’N, and longitudes 87°09’25’’E to 87°15’32’’E. The elevation of the basin ranges from 60 meters above sea level (masl) on the alluvial plains in India to more than 8,000 masl in the High Himalayas in Nepal. Due to the large variation in elevation, the river basins of the Himalayan region can be divided into four ecological regions: Indo-Gangetic Plains (60-200 masl), hills (200-4,000 masl), mountains (> 4,000 masl), and the transmountain region, which lies north of the Himalayan mountain range and extends into China (Figure 2). The climate of the Koshi Basin ranges from tropical in the Gangetic Plains to alpine conditions in the high-altitude areas (Agarwal et al. 2014; Bharati et al. 2014, 2016).

Past Water Resource Assessments and Climate Change Studies in the Koshi Basin and Eastern Himalayas

Recently, there has been an increase in the number of publications on the Koshi Basin in relation to future CC and its impacts on water availability, runoff components, crop production and natural hazards, using historical trend analysis and IPCC projections. One of the first studies in the Koshi

Basin was carried out by Sharma et al. (2000), who studied basin-wide land use, and climatic and hydrological trends. The analysis of climatic and hydrological trends from 1947 to 1993 indicated an increasing trend for temperature and precipitation but a decreasing trend in the discharge, which is more significant in low-flow months. Shrestha et al. (2013) assessed the spatial and temporal impacts of CC on rice–wheat cropping systems, focusing on Irrigation Water Requirement (IWR) in the Bagmati River Basin (a sub-basin of the Koshi Basin). The study found that the impact of CC on IWR depends on different physiographic regions as well as the growth stages of rice and wheat. Due to the migration of people, IWR is decreasing in the hills and mountain but increasing in the Terai Plains. Therefore, there will be increased pressure on large-scale irrigation systems in the Terai. Qi and Redman (1993) conducted a climatic linear trend analysis using 40 years of climate data from 10 meteorological stations and showed a warming trend of 0.25 °C per decade. Bhatt et al. (2014) also investigated climate trends and the impacts on crop production. The results showed warming trends in most parts of the basin with an increase in mean monthly temperature from 1960-2008, which then has a negative impact on the crop yields (rice, maize and wheat). Crop yields, however, might benefit from higher temperatures provided that other conditions such as water availability and soil fertility are favorable (Bhatt et al. 2014). More recently, Nepal (2016) assessed historical records of precipitation and temperature trends in the Nepal part of the Koshi Basin using data from the last 40 to 50 years. The study suggested that about two-thirds of the precipitation stations (22 out of 36) show increasing trends, of which only two were statistically significant, and 14 show decreasing trends, of which only one was statistically significant. Similarly, the maximum temperature increased at the rate of 0.058 °C per year based on data from the last 40 years (Nepal 2016). Furthermore, Lacombe and McCartney (2014) conducted statistical assessments and found that increasing temperatures in the Indian Himalayan region are likely affecting the monsoon and hence changing precipitation patterns in the north of the country.

There have also been a few publications using projected CC data. Agarwal et al. (2014) analyzed precipitation using outputs from 10 General Circulation Models (GCMs) under three IPCC emission scenarios (B1, A1B and A2) for three future periods (2020s, 2055s and 2090s) and for six physiographic regions in the Koshi Basin. Results from the study indicate that not all 10 GCMs agree that changes in precipitation will be positive or negative. A majority of the GCMs and the average values of all the GCMs for each scenario indicate a positive change in summer, autumn and annual precipitation but a negative change in spring precipitation. Differences in the GCM projections exist for all the three future periods and the differences increase with time. The estimated uncertainty is higher for scenario A1B than for scenarios B1 and A2. Agarwal et al. (2016) suggested that the temperature of the Koshi Basin is expected to rise with a relatively higher increase in the mountains than in the hills based on data obtained from 10 GCMs under B1, A1B and A2 scenarios. Khadka et al. (2014) predicted future changes in climatic parameters of the Tamakoshi Basin, one of the highly glaciated sub-basins of the Koshi Basin. The GCMs used in the analysis indicate that both temperature and precipitation will increase by 0.025 °C/year and 4.7 mm/year, respectively. Bharati et al. (2014, 2016) stated that the impacts of CC are scale dependent. The impacts of CC are more noticeable at sub-basin and seasonal scales rather than at annual, full basin scales. Therefore, storage and transfer of water from water-surplus seasons and areas to water-deficit seasons and areas are good adaptation strategies. Furthermore, as variability in the system is also likely to increase, future strategies should aim at dealing with variability as well as uncertainty, instead of focusing on changes in average trends. Devkota and Gyawali (2015) assessed CC impacts based on two regional climate models (PRECIS-HADCM3Q0 and PRECIS-ECHAM05). The results showed that CC does not pose a major threat to average water availability. However, temporal flow variations are expected to increase in the future. The magnitude of projected

flow for given return periods strongly depends on the climate model run considered. The ECHAM05 results show greater flow changes than those estimated from the HADCM3 model. Gosain et al. (2006) predicted increases in rainfall, evapotranspiration (ET), snowmelt and surface runoff due to CC for the Koshi Basin, but they did not assess seasonal and spatial variations at sub-basin level. Nepal (2016) used the process-based J2000 hydrological model in the Dudh Kohsi sub-catchment and applied the A1B scenarios of the PRECIS regional climate model until the end of the century. The study indicated that runoff may increase by 13% followed by a slight decrease by the end of the century compared to the reference period. The increase in runoff is attributed to the increase in precipitation in the future. Similarly, ET may increase by 16% by the end of the century.

FIGURE 2. A map showing the Land Use/Land Cover (LULC) patterns across the four ecological regions in the Koshi Basin.

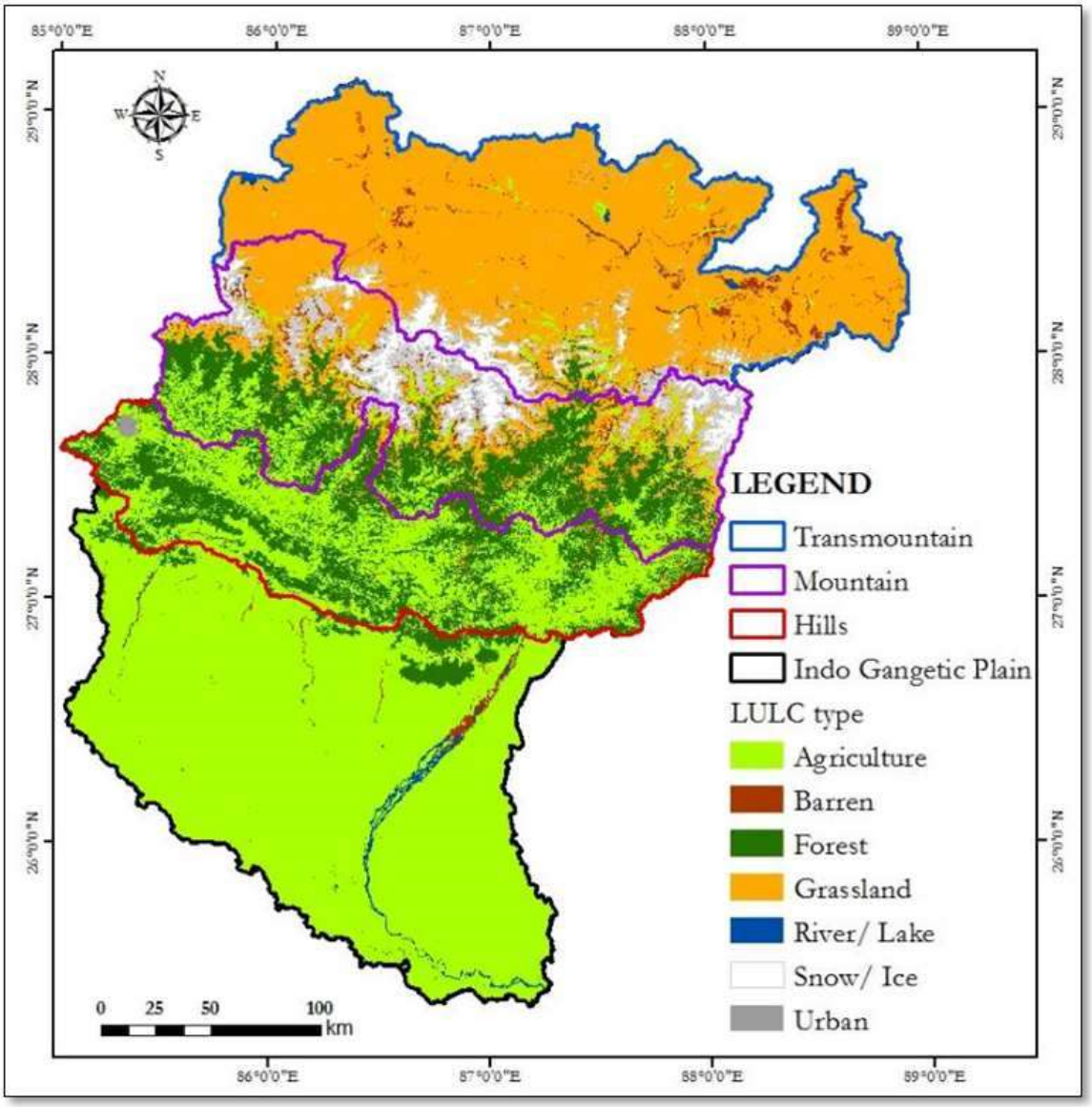

Furthermore, snowmelt and glacier melt are major contributors to runoff and streamflow in Himalayan basins (Immerzeel et al. 2013; Nepal 2016). According to Khadka et al. (2014), the average annual contribution of snowmelt during the reference period (2000-2008) in Tamakoshi is around 17.7%. Similarly, Nepal (2016) estimated a 17% glacier contribution from the Dudh Koshi Basin (the neighboring catchment of Tamakoshi to the east). The study highlighted that the seasonal contribution is more important than the annual contribution. Similarly, Lutz et al. (2014) also estimated the glacier melt contribution to be about 19% in the Dudh Koshi Basin. In the Tamor catchment of the Koshi Basin, the snowmelt contribution to total runoff in the basin is reported to be about 29% on average. It is observed that the snowmelt contribution will not change significantly (17.8% in the 2020s to 17.3% in the 2050s). However, the rainfall contribution is projected to increase. Miller et al. (2012) also studied glacier meltwater contribution in the Hindu Kush Himalaya. The results showed that the impacts of glacier melt strongly affect flows in headwater catchments, but their effects decrease further downstream. Immerzeel et al. (2013) used results from the latest ensemble of GCMs analyzing climate scenarios – Representative Concentration Pathways (RCPs) 4.5 and 8.5 – to assess the hydrological impacts of CC in two Himalayan watersheds, i.e., the Baltoro (a part of the Indus system) and Langtang (a part of the larger Koshi Basin and Ganges system). The study projected an increase in precipitation and temperature in the Ganges Basin, and an increase in future runoff in both watersheds. The study also showed that, in both cases, glaciers will recede but net glacier melt runoff will increase until 2050. Therefore, in combination with a positive change in precipitation, water availability during this century is not likely to decline (Immerzeel et al. 2013). In a similar study, Lutz et al. (2014) used the latest ensemble of climate models and large-scale, high-resolution cryospheric-hydrological models to quantify the upstream hydrological regime of the Eastern Himalayas and the impacts of CC on future water availability. Their results showed an increase in precipitation for the Koshi Basin during the monsoon season. Specifically for the Koshi Basin, the study indicated that discharge might increase, at a higher magnitude during the monsoon season, at least up to 2050, primarily due to an increase in precipitation. Nonetheless, the nature of the hydrograph remains largely unaffected. However, the study also highlighted uncertainties in the results as well as large variations between the annual average and seasonal projections.

METHODS AND DATA

The methodological framework for this study is shown in Figure 3. Spatial and time-series data from the basin were collected and used to set up the SWAT model. The model was then calibrated and validated to observed flow data from multiple stations in Nepal (Table 1) using different criteria such as coefficient of determination (R^2), Nash-Sutcliffe Efficiency (NSE) and bias. Flow data from India and China would increase model reliability, but as these data are not accessible, only flow data from Nepal were used. This is still the most detailed model of the Koshi Basin to date. The model results were then analyzed in terms of water balances at daily scales per sub-basin, and compared to model runs using CC projection data to evaluate possible impacts from modelled climate change. Details of each methodological step as well as the SWAT model are described in the following sections.

FIGURE 3. Methodological framework for this study.

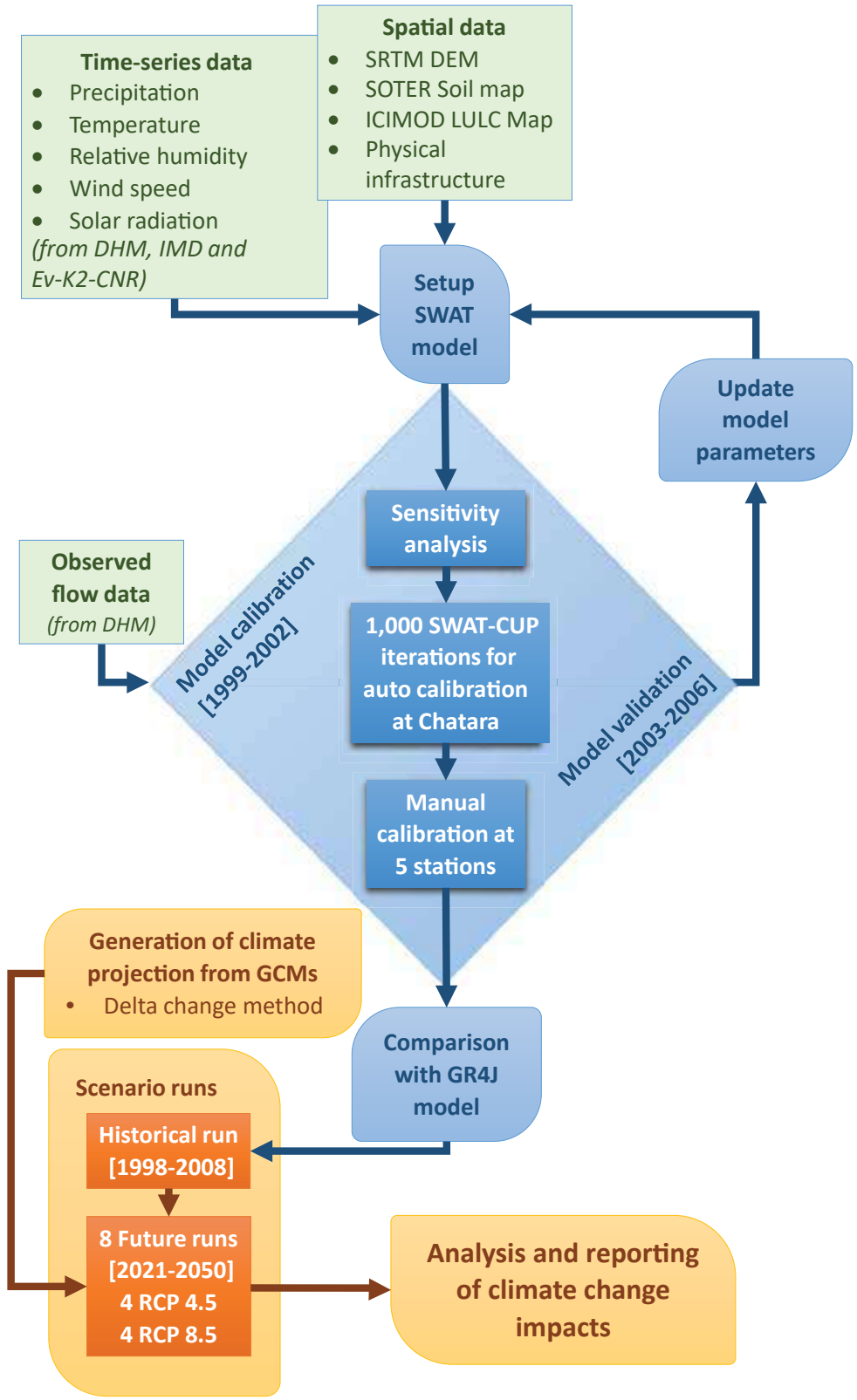

Notes: DEM – Digital elevation model; LULC – Land use/land cover; SWAT – Soil and Water Assessment Tool; CC – Climate change; DHM – Department of Hydrology and Meteorology; SRTM – Shuttle Radar Topography Mission; SOTER – Soil and Terrain database system; ICIMOD – International Centre for Integrated Mountain Development; GCM – General Circulation Model; IMD - India Meteorological Department.

TABLE 1. An overview of the main datasets.

Category	Data	Data source
Hydrology	River discharge	Department of Hydrology and Meteorology (DHM), Nepal
Climate	Precipitation, temperature, relative humidity, solar radiation, wind speed	For Nepal, DHM and Ev-K2-CNR (Chartered Association in Nepal) station data were used; for China, TRMM and Climate Forecast System Reanalysis (CFSR) gridded data were used; for India, India Meteorological Department (IMD) gridded and point data were used
Topography	Digital elevation model (DEM) - 90 m resolution	Shuttle Radar Topography Mission (SRTM)
Soils	Soil map and soil properties	Soil and Terrain database system (SOTER) soil map of China, Nepal and Indo-Gangetic Plains. Downloaded from ISRIC – World Soil Information website (https://www.isric.org/)
Land use	Land use map	Land cover types of the land use/land cover (LULC) map is based on the map received from the International Centre for Integrated Mountain Development (ICIMOD), and sub-classes for the irrigated land are based on the district-wise crop types and cropping calendar of China, Nepal and India
Physical infrastructure	Dams, barrages, irrigation systems	Google Earth, Japan International Cooperation Agency (JICA) 1986, and Department of Irrigation, Nepal, reports and other internet sources such as Indiastat (https://www.indiastat.com/)

Soil and Water Assessment Tool (SWAT)

SWAT is a process-based hydrological model that predicts the impact of land management practices on water, sediment and agricultural chemical yields in complex basins with varying soils, land use and management conditions (Arnold et al. 1998; Srinivasan et al. 1998). The main components of the model include climate, hydrology, erosion, soil temperature, plant growth, nutrients, pesticides, land management, and channel and reservoir routing.

Conceptually, SWAT divides a basin into sub-basins. Each sub-basin is connected through a stream channel and further divided into Hydrologic Response Units (HRUs). An HRU is a unique combination of a soil and vegetation type in a sub-watershed. SWAT simulates hydrology, vegetation growth and management practices at the HRU level. The hydrologic cycle, as simulated by SWAT, is based on the water balance equation:

$$SW_t = SW_o + \sum_{i=1}^{n} (R_{day} - Q_{surf} - E_a - w_{seep} - Q_{gw}) \quad (1)$$

Where:

SW_t : Final soil water content (mm)
SW_o : Initial soil water content (mm)
t : Time in days
R_{day} : Amount of precipitation on day i (mm)

Q_{surf} : Amount of surface runoff on day i (mm)
E_a : Amount of evapotranspiration on day i (mm)
w_{seep} : Amount of percolation on day i (mm)
Q_{gw} : Amount of return flow on day i (mm)

Since the model maintains a continuous water balance, the subdivision of the basin enables the model to reflect differences in evapotranspiration for various crops and soils. Thus, runoff is predicted separately for each sub-basin and routed to obtain the total runoff for the basin. This increases the accuracy and gives a much better physical description of the water balance. More detailed descriptions of the model can be found in Arnold et al. (1998) and Srinivasan et al. (1998). The physical infrastructure was included in the model using the reservoir module in SWAT.

Spatial Data

SWAT requires three basic types of data for delineating the basin into sub-basins and HRUs, i.e., a DEM, soil map and a land cover map. The SRTM 90 m resolution DEM for the basin was used as input to the model. The stream network was also generated using the SRTM 90 m DEM. The generated stream network was then compared with the **Hydro**logical data and maps based on **SH**uttle **E**levation **D**erivatives at multiple **S**cales (HydroSHEDS) (http://hydrosheds.cr.usgs.gov/index.php) river network (15 second spatial resolution) as well as Google Earth images in order to rectify some errors. Based on the Google Earth images, incorrect locations of some parts of the generated river network (especially the main branches) were corrected using the burning process in geographic information systems (GIS). The basin was subdivided into 127 sub-basins.
The basic LULC map used in the model was obtained from the International Centre for Integrated Mountain Development (ICIMOD) (http://geoportal.icimod.org/) and contained 15 major LULC classes. However, as agricultural land was not subdivided into irrigated and rain-fed land, the agricultural area was further subdivided into irrigated and rain-fed areas using the GlobCover 2009 map (http://due.esrin.esa.int/page_globcover.php). Further, the irrigated and rain-fed areas were discretized to district level for China, Nepal and India within the Koshi Basin with major crop types. The district-wise crop types and calendar were entered into the SWAT model through its management schedule capabilities, which involves input of information on the planting or growing season of plants, irrigation operation, etc. A large part of the study basin is agricultural land (38,614 km^2) followed by grassland (21,599 km^2). Snow and glaciers cover an area of 5,232 km^2.
The soil and terrain database system (SOTER) soil map of China, Nepal and Indo-Gangetic Plains was downloaded from the ISRIC website (https://www.isric.org/). The soil nomenclature was based on FAO and ISRIC (1990); based on the processed map, there are 37 classes. The dominant soil is Gelic Leptosols in the transmountain and mountain region, Eutric Cambisols in the hills, and Eutric Gleysols and Eutric Cambisols in the Terai and Indo-Gangetic Plains of the basin.

Time Series Data

SWAT requires time series of observed climate data, i.e., rainfall, minimum and maximum temperatures, sunshine duration, wind speed and relative humidity. Table 2 lists the number of climate stations used for modeling while the locations of these stations are presented in Figure 4. Daily observed climate and hydrological data were collected from the Department of Hydrology and Meteorology (DHM), Nepal, and India Meteorological Department (IMD). However, as it

was not possible to access data from the Chinese part of the Koshi Basin and as there are no climate stations in the higher altitude areas in Nepal, precipitation data from the TRMM (http://trmm.gsfc.nasa.gov/) were used. In addition, data (daily rainfall, temperature, wind speed, solar radiation and humidity) from three Ev-K2-CNR (http://www.evk2cnr.org/cms/en) stations in the Himalayan Region and Climate Forecast System Reanalysis (CFSR) gridded data for China were also acquired and used in the model.

TABLE 2. Summary of climate and hydrological data, and climate stations used for modeling.

Description	Remarks
Climate data (daily)	
• 92 Precipitation stations • 53 Temperature stations • 55 Humidity stations • 56 Wind speed stations • 68 Solar duration stations	• Includes data from DHM (Nepal), IMD (India), Ev-K2-CNR, TRMM and CFSR • Compilation of both point (station) and gridded data
Hydrological data (daily)	
• 40 hydrological stations	All from DHM (Nepal); five stations used for calibration and validation

FIGURE 4. Hydrological, meteorological and calibration stations in the Koshi Basin.

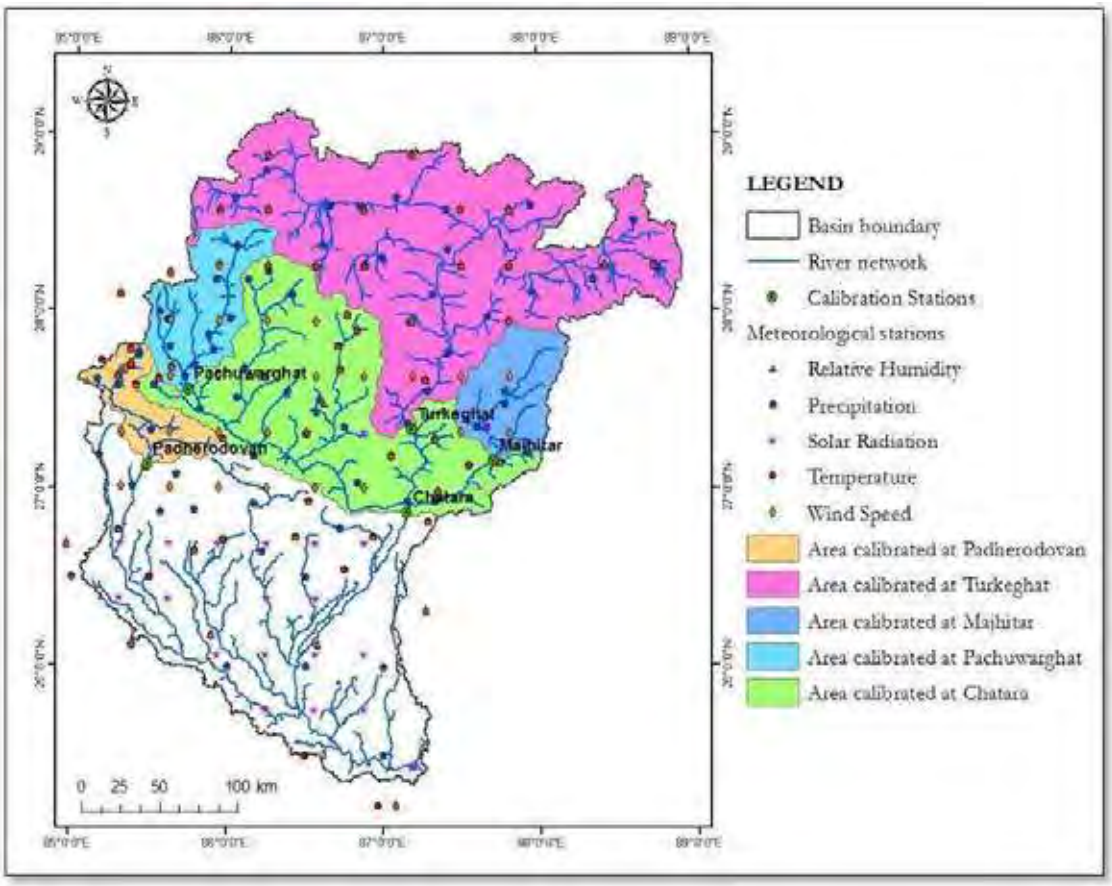

Model Calibration and Validation

The model was calibrated using daily flow data from 1999 to 2002 and validated for 2003 to 2006. This period was used so that it matches the land cover map chosen for the basin. The measured flow data for this period was also more complete. Calibration of the model was carried out in three steps: sensitivity analysis, auto calibration and manual calibration. Sensitivity analysis was performed using the built-in tool of SWAT, changing the values one at a time, from which the ten most sensitive parameters were identified. Table 3 lists out these parameters with their ranking, i.e., 1 is the most sensitive and 10 the least sensitive. The most sensitive parameters are related to the baseflow process (ALPHA_BF - baseflow recession factor, GWQMN - threshold depth of water in aquifer, REVAPMN - threshold depth of water in aquifer for percolation/evaporation) and surface runoff (CN2 - curve number, ESCO - soil evaporation compensation factor, SURLAG - surface runoff lag coefficient). The built-in tool of SWAT and SWAT-CUP was used for auto calibration using these parameters. The model was run for 1,000 iterations during this step. Sensitivity analysis in SWAT and auto calibration using SWAT and SWAT-CUP are limited to the use of observed data from a single gauging station. Thus, observed flow data from Chatara (outlet of the 96th sub-basin) were used for this purpose. Although the range of values for the sensitive parameters was narrowed down (Table 3), the simulated and observed hydrographs did not match well. One obvious reason could be the large size of the basin and hence the inability to fit the parameters over the entire basin based on the results from one flow station. Therefore, it was necessary to also perform manual calibration.

TABLE 3. Initial values of the parameters after sensitivity analysis and auto calibration.

Sensitivity analysis ranking	Parameters*	Initial value suggested by SWAT
1	ALPHA_BF	0.54
2	CH_K2	142.79
3	CH_N2	0.1001
4	CN2	19.129
5	ESCO	0.6208
6	GWQMN	944.35
7	REVAPMN	8.967
8	SOL_AWC	18.17
9	SOL_K	23.45
10	SURLAG	2.35

Note: * For detailed explanation of the parameters, please refer to Arnold et al. 2011.

Manual calibration was done simultaneously using the daily flow data at five gauging stations, all established and maintained by DHM within Nepal. Unfortunately, flow data from China and India were not available. An iterative approach was used for manual calculation which comprised the following steps: (i) simulation; (ii) comparison of observed and simulated values; (iii) checking whether the output is reasonable; (iv) if not, adjusting the parameters based on expert judgment; and (v) repetition of the process until the best results are obtained (Arnold et al. 2012). It was found rational to calibrate the major tributaries of the Koshi River independently to incorporate the spatial variability of the basin in the model. Figure 4 shows the Arun, Tamor, Sunkoshi, Bagmati and Saptakoshi rivers along with the Turkeghat, Majhitar, Pachuwarghat, Padherodovan and Chatara gauging stations, respectively, used for calibration and

validation. During manual calibration, first, adjustments were made to those parameters which were deemed most sensitive during the sensitivity analysis for the Chatara gauging station, as discussed previously, followed by adjustments to the parameters deemed to be least sensitive. For some catchments, additional parameters that were not identified during the sensitivity analysis were adjusted for better performance of the model. During calibration, parameters were varied within a reasonable range (Table 4). Furthermore, visual inspection of the hydrographs (peak, time to peak, shape of the hydrograph and baseflow), statistics (mean, standard deviation [SD], coefficient of determination [R^2], Nash-Sutcliffe Efficiency [NSE], percent bias [PBIAS] and root mean square error [RMSE]-observations standard deviation ratio [RSR]) and comparison of the simulated water balance with the observed values were the basis for evaluating model prediction during manual calibration.

Table 4 shows that the most sensitive parameters, such as runoff curve number (CN_2), groundwater delay (GW_DELAY) and baseflow recession factor (ALPHA_BF), were common calibration parameters at all the stations. Use of initial SWAT-estimated parameters mostly underestimated the baseflow in all cases. Therefore, CN_2 had a key role in increasing the infiltration and hence the groundwater flow into the stream. Similarly, the value of GW_ DELAY was maintained within 90-120 days as it represents the delay in the groundwater flow contributing to the baseflow. It is to be noted that, in the Koshi Basin, around 80% of the total annual precipitation occurs in 4 months (June-September) and the baseflow during the dry period (remaining 8 months) is sustained by the groundwater recharge during the monsoon season. The value of ALPHA_BF was changed depending on the slope of the receding limb of the hydrograph. Other flow-related parameters, such as soil evaporation compensation factor (ESCO), revap coefficient (GW_REVAP), threshold depth of water in the shallow aquifer required for return flow to occur (GWQMN), soil depth (SOL_Z), available water capacity of the soil (SOL_AWC), saturated hydraulic conductivity (SOL_K), effective hydraulic conductivity in the main channel (CH_K2), channel Manning's number (CH_N2) and surface runoff lag coefficient (SURLAG) were adjusted from initial estimates to match the simulated and observed flows. As elevation bands were used in the model, TLAPS and PLAPS played an important role in the spatial distribution of temperature and precipitation (Rahman et al. 2013). Snow/glacier-related parameters, such as TLAPS, lateral flow travel time (LATTIME), snowfall temperature (SFTMP) and snowmelt base temperature (SMTMP) were also adjusted in certain sub-basins where snow/ glacier coverage is large.

Once the model was calibrated, it was run for validation in a different time period, i.e., from 2003 to 2006, using the same parameter sets obtained during calibration. The streamflow results are compared for gauged data for 2003-2006 using the same statistical measures as in the calibration process. The purpose of this step is to assess whether the model can reproduce the flow in this period, thereby providing a measure of its robustness.

Tables 5 and 6 show the daily and monthly statistics of calibration and validation, respectively, at the five gauging stations. Figures 5 to 9 show the observed and simulated daily hydrographs at the five gauging stations. The overall performance of the model was satisfactory. The differences in the mean and SD of the observed and simulated datasets are within ±15% and 20% on daily runs except for Turkeghat and Padherodovan. Similarly, NSE at the daily time step is greater than 0.65 for the calibration period and greater than 0.58 for the validation period for all the gauging stations. Also, R^2 for the daily run is greater than 0.66 for both the calibration and validation periods at all the gauging stations. In the case of the monthly run (Table 6), NSE and R^2 are both well above 0.85 for the calibration period. For the validation period, R^2 is greater than 0.85 for all the stations except Turkeghat (0.75) and NSE is above 0.8 for all the stations except Turkeghat (0.66).

TABLE 4. Calibrated SWAT parameters.

	Flow station	Parameters*	File*	Level*	Initial values	Calibrated values	Range*
1	Turkeghat	TLAPS	.sub	Sub-basin	-5.6	-3.8	0 - -10
		PLAPS	.sub	Sub-basin	-50	5.8	0 - 100
		CN_2	.mgt	HRU	Varies	0.8 (Ratio)	35 - 98
		SOL_K	.sol	HRU	Varies	0.8 (Ratio)	0 - 100
		GW_DELAY	.gw	HRU	31	120	0 - 50
		ALPHA_BF	.gw	HRU	0.048	0.55	0 - 1
		ESCO	.hru	HRU	0	0.7	0 - 1
		LATTIME	.hru	HRU	1	1	0 - 180
		SOL_Z	.sol	HRU	300	600	0 - 3,000
		GWQMN	.gw	HRU	0	550	0 - 5,000
		SURLAG	.bsn	Basin	10	1	1 - 10
		SFTMP	.bsn	Basin	1	1	-5 - 5
		SMTMP	.bsn	Basin	0.5	0.9	-5 - 5
2	Majhitar	GW_DELAY	.gw	HRU	31	85	0 - 50
		CN_2	.mgt	HRU	Varies	0.8 (Ratio)	35 - 98
		ESCO	.hru	HRU	0	0.5	0 - 1
		SOL_Z	.sol	HRU	300	800	0 - 3,000
		SOL_K	.sol	HRU	Varies	0.75 (Ratio)	0 - 100
		SOL_AWC	.sol	HRU	Varies	0.95 (Ratio)	0 - 1
		GWQMN	.gw	HRU	0	415	0 - 5,000
		CH_N2	.rte	Reach	0.014	0.035	0 - 1
3	Pachuwarghat	CN_2	.mgt	HRU	Varies	0.75 (Ratio)	35 - 98
		GW_DELAY	.gw	HRU	31	90	0 - 50
		ALPHA_BF	.gw	HRU	0.048	0.09	0 - 1
		GWQMN	.gw	HRU	0	500	0 - 5,000
		SOL_Z	.sol	HRU	300	600	0 - 3,000
		SOL_K	.sol	HRU	Varies	0.7 (Ratio)	0 - 100
		SOL_AWC	.sol	HRU	Varies	1.167 (Ratio)	0 - 1
		ESCO	.hru	HRU	0	0.7	0 - 1
4	Padherodovan	CN_2	.mgt	HRU	Varies	1.35 (Ratio)	35 - 98
		GW_DELAY	.gw	HRU	31	90	0 - 50
		ALPHA_BF	.gw	HRU	0.048	0.015	0 - 1
		SOL_AWC	.sol	HRU	Varies	1.135 (Ratio)	0 - 1
		SOL_K	.sol	HRU	Varies	0.56 (Ratio)	0 - 100
		ESCO	.hru	HRU	0	0.075	0 - 1
		GW_REVAP	.gw	HRU	0.02	0.05	0.02 - 0.2
		CH_K2	.rte	Reach	0	6.21	0 - 150
		CH_N2	.rte	Reach	0.014	0.211	0 - 1
5	Chatara	GW_DELAY	.gw	HRU	31	100	0 - 50
		ALPHA_BF	.gw	HRU	0.048	0.5	0 - 1
		CN_2	.mgt	HRU	Varies	0.65 (Ratio)	35 - 98
		LATTIME	.hru	HRU	1	4	0 - 180

Note: * For detailed explanation of the parameters, please refer to Arnold et al. 2011.

Although PBIAS for the calibration period is well within the ±10% range at all the stations, the values are slightly higher in the validation period at Turkeghat (25.01%), Padherodovan (-45.52%) and Chatara (13.77%). Santhi et al. (2001) have identified potential errors (spatial variability errors in rainfall, soils and land use, errors in measuring flow and errors caused by sampling strategies) that can occur in the measured input data and data used for calibration. As a very large area from Tibet contributes to the flow at Turkeghat, it is strongly dependent on the input (precipitation) data within its catchment area. The TRMM-gridded data in this part of the basin were used due to the unavailability of observed data. Also, accurate information on the snow and glaciers regarding their coverage area, depth and depletion rate was not available for the areas at high altitudes. Thus, the low values of the statistics in this sub-basin are most likely attributable to the precipitation and snow/glacier input data. In addition to the above statistical indices, the ratio of the root mean square error to the standard deviation of measured data (RSR) was also calculated which includes a scaling/normalization factor. RSR varies from zero to a large positive value. The lower the RSR, lower the RMSE and better the model simulation performance (Moriasi et al. 2007). RSR at all stations was found to be less than 0.4 for the calibration period and less than 0.6 for the validation period in the monthly run. Based on the general performance ratings criteria developed by Moriasi et al. (2007) for a monthly time step, it can be seen that the calibration and validation results are “very good” in almost all cases (Table 6). Figures 5 to 9 show daily observed and simulated flows from the calibration stations. The model simulations improve for the lower part of the basin as can be seen from the figure for the station at Chatara (Figure 9).

TABLE 5. Daily calibration and validation statistics assessing model performance at five hydrological stations.

River	Station (index number)	Index	Calibration	Validation
Arun	Turkeghat (#604.5)	R^2	0.81	0.64
		NSE	0.81	0.58
		PBIAS %	-6.81	24.6
		RSR	0.44	0.65
Tamor	Majhitar (#684)	R^2	0.66	0.67
		NSE	0.65	0.58
		PBIAS %	7.52	-3.65
		RSR	0.59	0.66
Sunkoshi	Pachuwarghat (#630)	R^2	0.74	0.71
		NSE	0.72	0.65
		PBIAS %	-2.06	5.42
		RSR	0.53	0.59
Bagmati	Padherodovan (#589)	R^2	0.71	0.70
		NSE	0.71	0.67
		PBIAS %	-7.89	-45.38
		RSR	0.54	0.57
Saptakoshi	Chatara (#695)	R^2	0.86	0.83
		NSE	0.85	0.80
		PBIAS %	-8.69	13.77
		RSR	0.39	0.44

TABLE 6. Monthly calibration and validation statistics assessing model performance at five hydrological stations.

River	Station (index number)	Index	Calibration	Validation
Arun	Turkeghat (#604.5)	R^2	0.95	0.75
		NSE	0.94	0.66
		PBIAS %	-6.86	25.01
		RSR	0.24	0.58
		*Performance	Very good	Satisfactory
Tamor	Majhitar (#684)	R^2	0.91	0.95
		NSE	0.85	0.95
		PBIAS %	7.41	-3.75
		RSR	0.38	0.22
		*Performance	Very good	Very good
Sunkoshi	Pachuwarghat (#630)	R^2	0.93	0.94
		NSE	0.93	0.93
		PBIAS %	-2.16	5.50
		RSR	0.26	0.26
		*Performance	Very good	Very good
Bagmati	Padherodovan (#589)	R^2	0.93	0.95
		NSE	0.92	0.82
		PBIAS %	-8.04	-45.52
		RSR	0.27	0.42
		*Performance	Very good	Unsatisfactory
Saptakoshi	Chatara (#695)	R^2	0.90	0.88
		NSE	0.89	0.84
		PBIAS %	-8.72	13.77
		RSR	0.32	0.40
		*Performance	Very good	Good

Note: * For details, please refer to Moriasi et al. 2007.

FIGURE 5. Observed and simulated flows at Turkeghat (#604.5) on a daily time step.

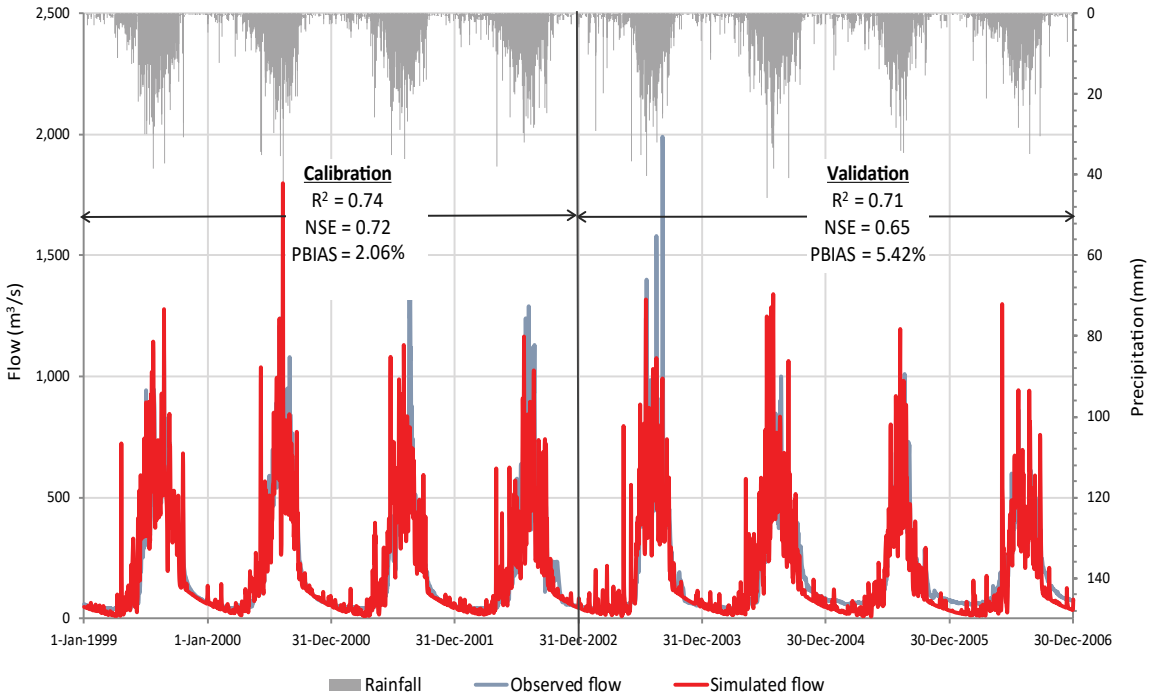

FIGURE 6. Observed and simulated flows at Majhitar (#684) on a daily time step.

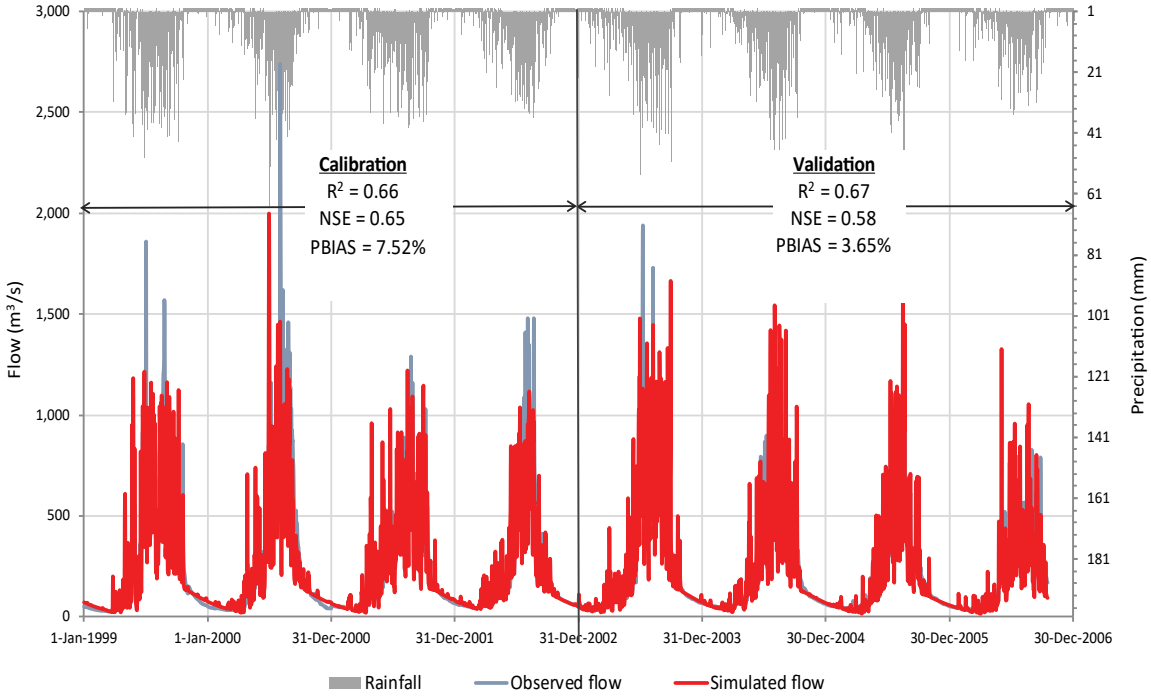

FIGURE 7. Observed and simulated flows at Pachuwarghat (#630) on a daily time step.

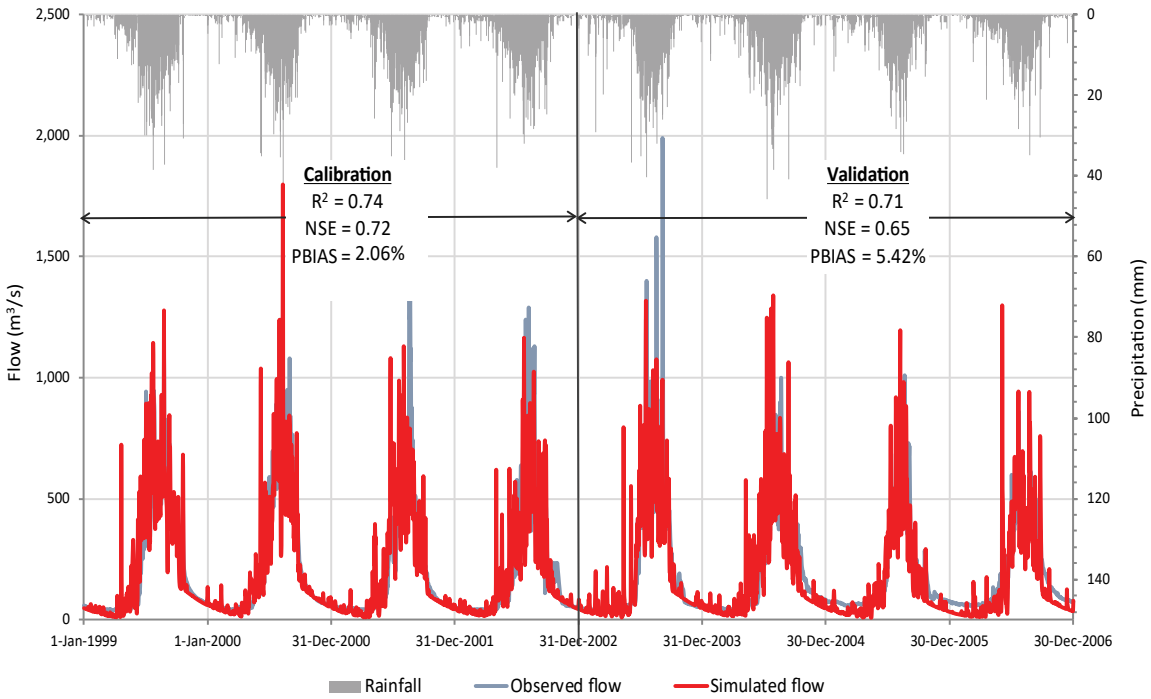

FIGURE 8. Observed and simulated flows at Padherodovan (#589) on a daily time step.

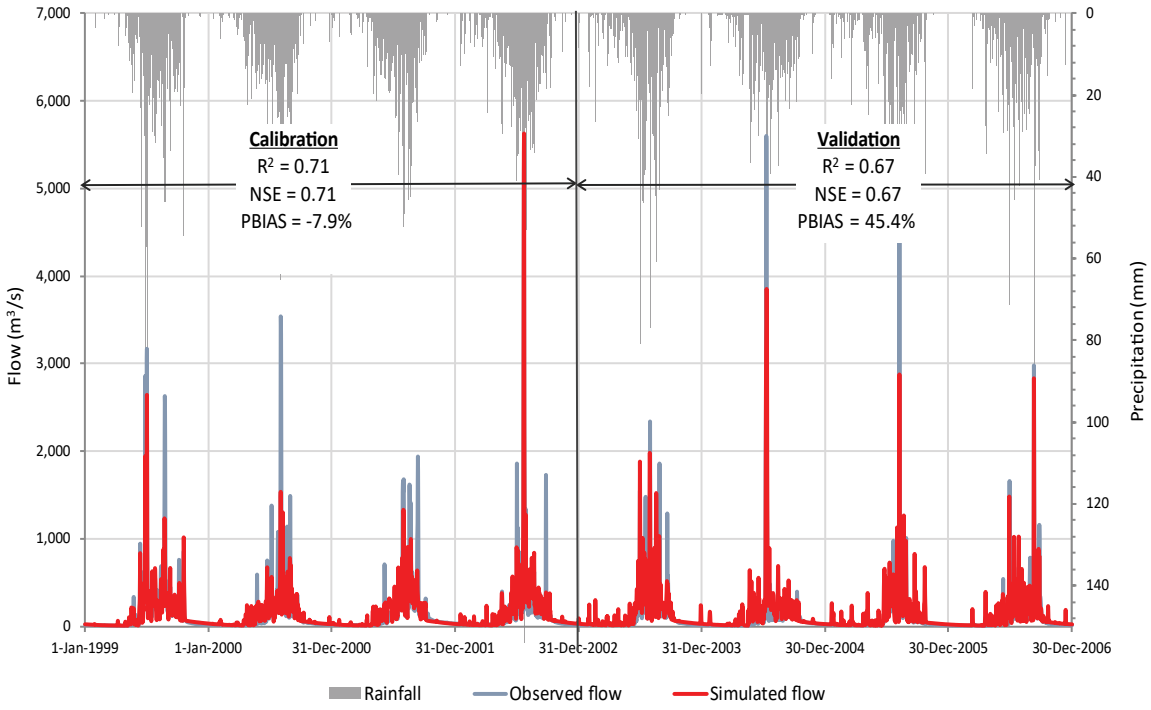

FIGURE 9. Observed and simulated flows at Chatara (#695) on a daily time step.

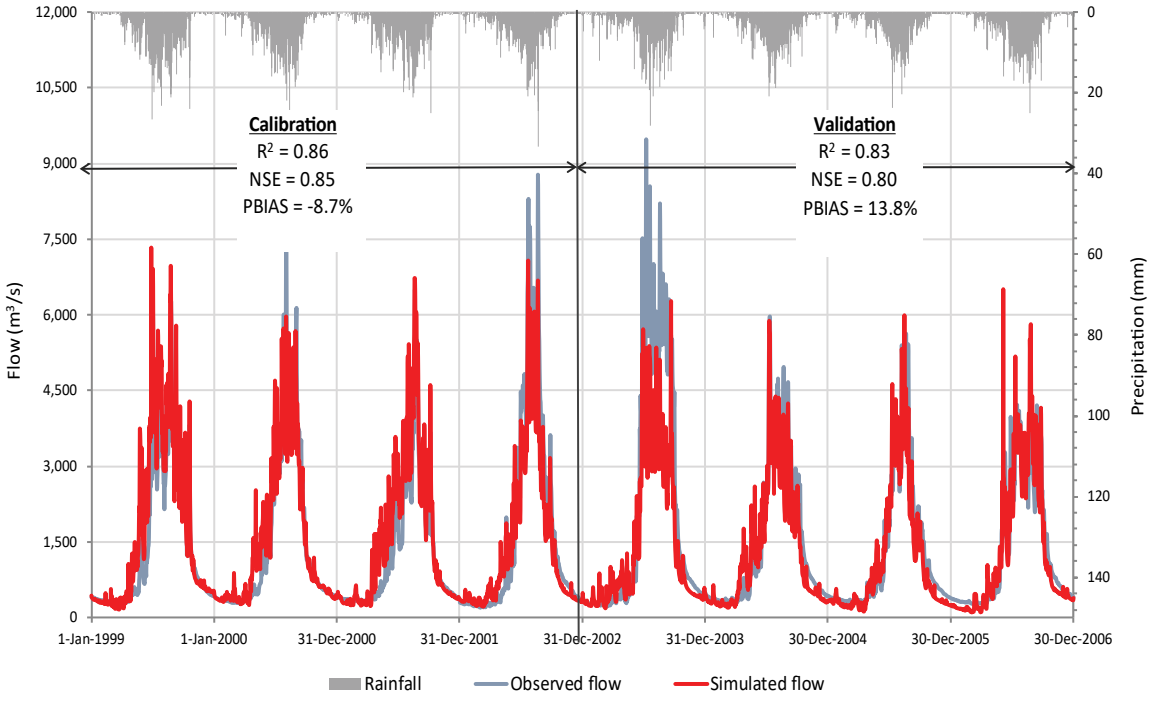

Comparison between GR4J and SWAT

The GR4J model developed by Perrin et al. (2003) is a daily lumped rainfall–runoff model. In this study, the outputs of the GR4J model were compared with the SWAT model outputs to compare the results between a complex semi-distributed model such as SWAT and a relatively simple conceptual GR4J model. Comparison of the results also helped to identify the robustness and uncertainties between the two modeling systems. Figure 10 presents the visual fit of the calibration and validation of the catchments in the Koshi Basin, with the GR4J set up. There is good agreement for all gauges. The model matches well for the rise, fall and recession of the hydrographs, but it tends to under-predict the peaks. The main discrepancies are the validation period for the Arun catchment, where the model under-predicts the streamflow, and the Bagmati catchment, where the model is unable to reproduce some very high flows.

FIGURE 10. 95% parameter prediction interval (grey shading) and time series of observed streamflow for the calibration (red dots) and validation (blue dots) periods for the Arun, Tamor, Sunkoshi, Bagmati and Saptakoshi hydrological stations.

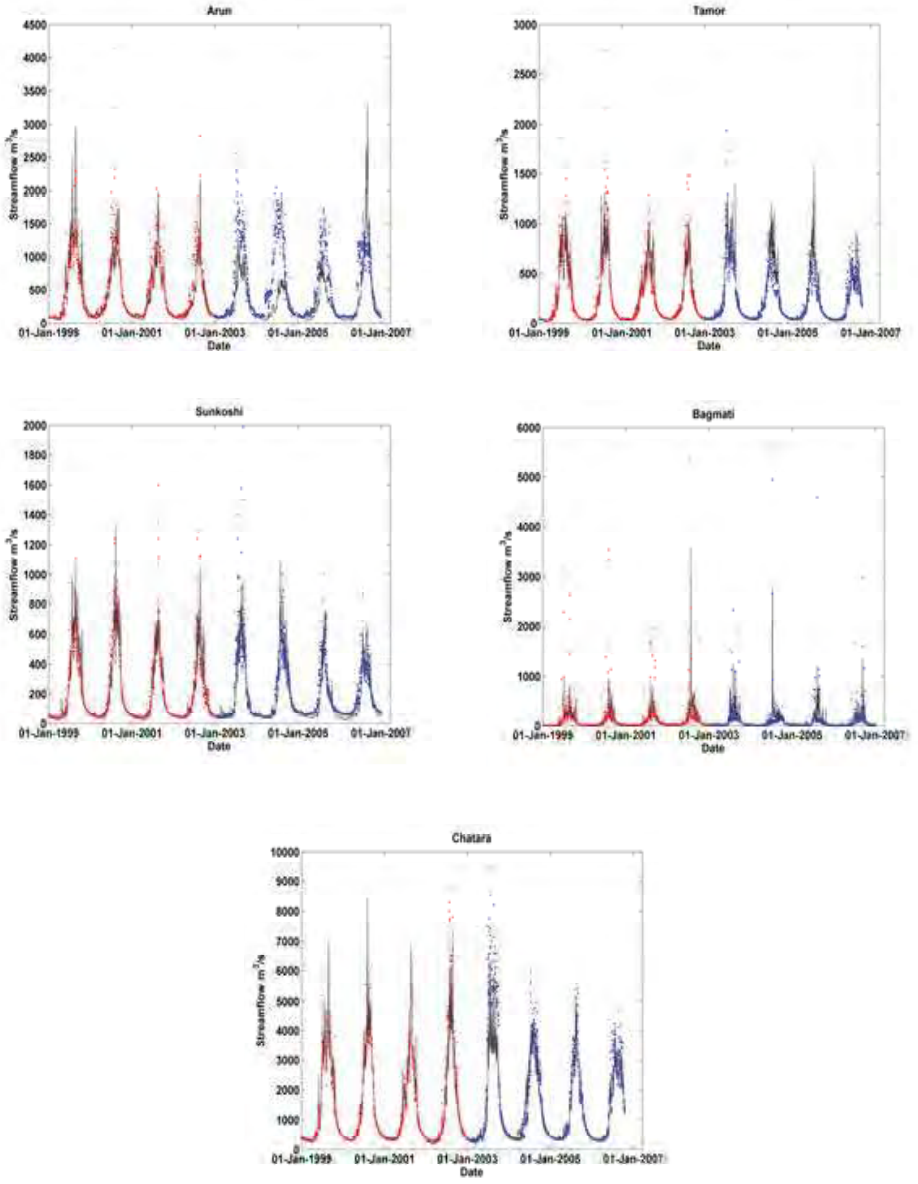

The performance statistics in Figure 11 and Table 7 indicate that the model performs well during calibration and validation for all catchments with the exception of the Bagmati catchment, where the NSE values for calibration are below 0.6 and the BIAS is also large with values of the order of 25%, as the model is unable to reproduce the large peaks and the volumes associated with them. However, across both calibration and validation in the Bagmati catchment, while showing lower NSE and R^2 values, the GR4J model tends to show lower biases across both periods.

Also, the model does not perform well at the Arun catchment, where it has a very large bias and a low NSE score during validation despite performing well during calibration. As mentioned in the SWAT results, the likely explanation for this poor performance lies with the rainfall data used in the model. For the period 2004-2005, the mean annual runoff was 60 mm higher than for the calibration period (1999-2002), but the mean annual rainfall is 300 mm lower. This would suggest that the large bias and poor NSE for the validation period is due to the discrepancy in rainfall. The lack of high resolution rainfall data could also be another hindrance to better model fit.

Table 7 also shows that the SWAT and GR4J models have similar performances, with GR4J showing better performance in terms of NSE for Tamor, Sunkoshi and Saptakoshi catchments, while SWAT is superior for the Arun and Bagmati catchments. On the other hand, in some catchments, SWAT has smaller biases than GR4J, but both models have similar problems for the Arun and Bagmati catchments.

TABLE 7. Comparison of results from the SWAT and GR4J models using R^2, NSE and BIAS (GR4J results correspond to the model results with highest NSE).

		Calibration		Validation	
Catchment	Statistic	SWAT	GR4J	SWAT	GR4J
Arun	R^2	0.81	0.79	0.67	0.45
	NSE	0.81	0.79	0.61	0.3
	BIAS	-6.8	5	25.8	38.4
Tamor	R^2	0.66	0.86	0.67	0.83
	NSE	0.65	0.86	0.58	0.75
	BIAS	7.5	3.8	-4.3	-10.7
Sunkoshi	R^2	0.74	0.87	0.71	0.81
	NSE	0.72	0.87	0.65	0.8
	BIAS	-2	1.9	5.4	10.8
Bagmati	R^2	0.71	0.64	0.7	0.6
	NSE	0.71	0.58	0.67	0.57
	BIAS	-7.9	21.5	-45.4	-1.9
Saptakoshi	R^2	0.86	0.93	0.83	0.91
	NSE	0.85	0.94	0.8	0.94
	BIAS	-8.7	1.9	13.77	15

FIGURE 11. Box plots of NSE (top panel) and percent bias (bottom panel) for calibration (left side) and validation (right side) for all five calibration gauges (Arun, Tamor, Saptakoshi, Bagmati and Sunkoshi).

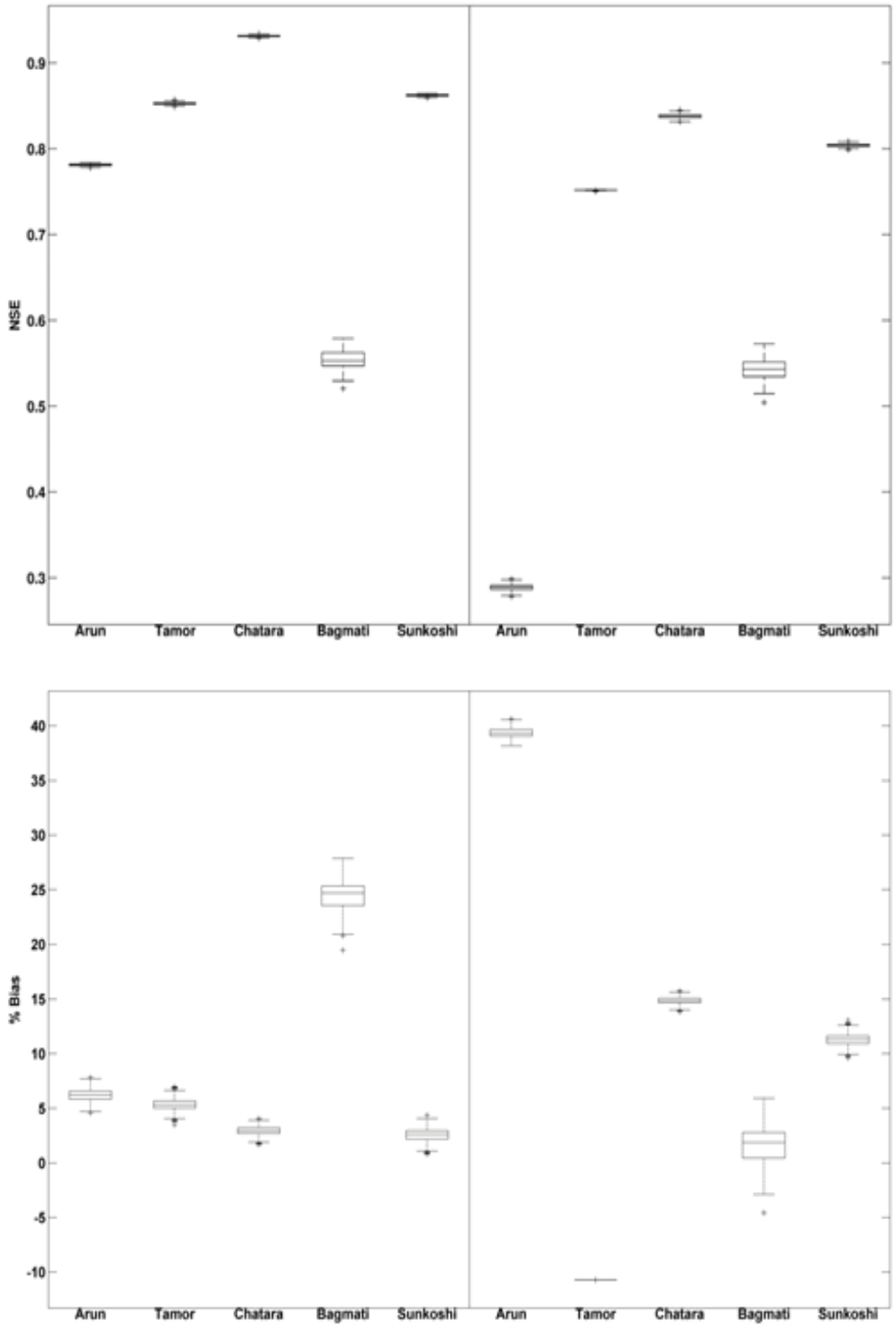

The posterior density as estimated by the DiffeRential Evolution Adaptive Metropolis (DREAM) (Vrugt et al. 2009) are shown in Figure 12. For most catchments, all parameters are well defined, with the exception of X1 (maximum capacity of production store) for the Saptakoshi catchment, X2 (groundwater exchange coefficient) for the Arun catchment, and X3 (routing store) for the Sunkoshi and Tamor catchments. In the cases of X1 and X3, the results indicate that larger values would be preferred. For the Arun catchment, however, the preference for a lower value of the groundwater exchange coefficient (X2) indicates that the model requires a good portion of the rainfall to be lost to groundwater. Therefore, it is possible that, for the calibration period, the rainfall is somewhat overestimated (suggesting a larger coefficient of runoff), and therefore a model calibrated to these excessive rainfall estimates exacerbates the problem when a lower rainfall estimate (such as in the years 2004-2005) is encountered. It is possible to calibrate the Arun model for the period 2003-2006 and obtain a PBIAS of only 1.8%, but the validation for the period 1999-2002 then shows an excess of streamflow resulting in a PBIAS of 45% (results not shown).

FIGURE 12. Posterior histograms for the four parameters of the GR4J hydrological model in each catchment (parameter bounds are X1 = [1,1500], X2 = [-10,5], X3 = [1,500], and X4 = [0.5,4]).

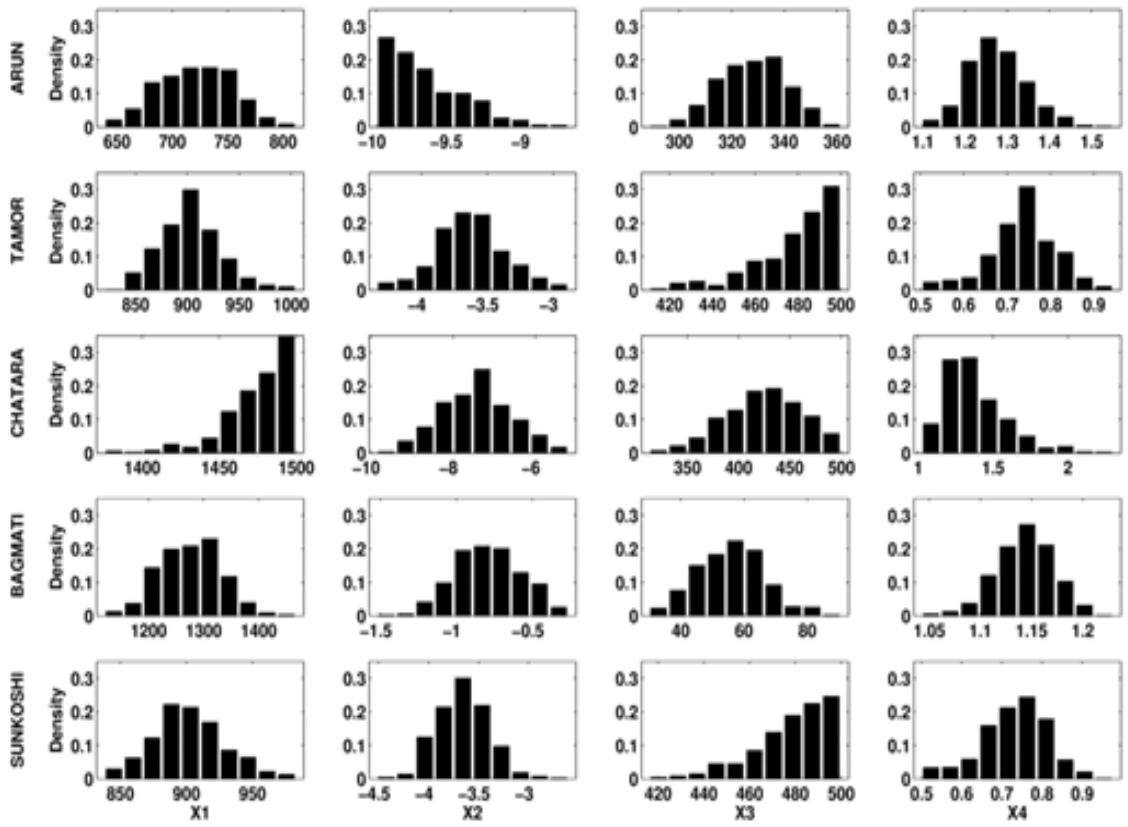

It is important to note that the uncertainties shown in Figure 12 are related to parameter uncertainty only, and do not take into account possible errors associated with model forcing (i.e., rainfall and evapotranspiration) and streamflow measurements. Of the five streamflow gauges considered here, the rating quality for three (Saptakoshi, Bagmati and Sunkoshi) from DHM, Nepal, is “fair”, while the quality is considered to be “good” for both Tamor and Arun catchments.

Capabilities and Limitations of the Model

As the calibration and validation statistics show satisfactory performance of the SWAT model in the hills and Terai of Nepal, the results obtained from these regions can be confidently used for further activities. Moreover, since agriculture covers a large area, especially in the plains of Nepal and India, the model results can also be used in the quantification of irrigation water, in particular. Land-use classes of the agricultural areas have been reclassified on a district-wise basis in order to extract information on the demand and use of water at the district level. Due to the unavailability of precipitation data and accurate information on snowmelt and glacier melt in the high mountainous areas of Tibet and Nepal, results from the model have a low confidence level for this region. Although the model performs all its calculations at a very small areal unit, it has not been developed and calibrated to simulate small catchments. Therefore, issues related to small sites/catchments should not depend solely on the model results.

It has been mentioned in the literature by the SWAT developers that its snow/glacier and groundwater component is not as strong as the surface hydrology component (Arnold et al. 1998). Thus, the use of other snow/glacier models and groundwater models is recommended, if these components are important and need to be analyzed in detail.

CLIMATE CHANGE SCENARIOS

In this study, delta change grids (Immerzeel et al. 2013) were used to downscale two Representative Concentration Pathways (RCPs) (RCPs 4.5 and 8.5), each scenario comprising four GCMs. The period of future simulations was 2021-2050; however, a period of 11 years (2040-2050) was used for climate change analysis.

The climate change scenarios considered in this model are two RCPs (RCPs 4.5 and 8.5). RCPs are a set of four new pathways developed for the climate modeling community as a basis for long-term and near-term modeling experiments. RCPs were developed from an innovative collaboration between integrated assessment modelers, climate modelers, terrestrial ecosystem modelers and emission inventory experts (van Vuuren et al. 2011). As shown in Table 8, the RCPs cover a period from 1850 to 2100 and the radiative forcing values of 2.6, 4.5, 6 and 8.5 Watts per square meter (W/m^2) (van Vuuren et al. 2011). The pathways selected for the study are RCP 4.5 (one of the medium stabilizing scenarios) and RCP 8.5 (a very high reference emission pathway).

TABLE 8. Overview of the representative concentration pathways (RCPs).

	Description
RCP 8.5	Rising radiative forcing pathways leading to 8.5 W/m² (~ 1,370 parts per million [ppm] carbon dioxide [CO_2]) by 2100. It is one very high reference emission scenario
RCP 6	Stabilization without overshoot pathway to 6 W/m² (~850 ppm CO_2) at stabilization after 2100
RCP 4.5	Stabilization without overshoot pathway to 4.5 W/m² (~650 ppm CO_2) at stabilization after 2100. It is a medium stabilizing scenario
RCP 2.6	Peak in radiative forcing at ~3 W/m² (~490 ppm CO_2) before 2100 and then declines to 2.6 W/m² by 2100

Source: van Vuuren et al. 2011.

Future Climate Data Generation

The climate change downscaling method involved selection of GCMs from a total of 43 model runs for RCP 4.5 and 41 model runs for RCP 8.5. The model selection was carried out as a part of a previous study by Lutz et al. (2014) for a larger domain of the Hindu Kush Himalayan (HKH) region. For each model run, the average annual difference in precipitation (%) and temperature (K) was determined (for the period 2021-2050 relative to 1961-1990). Based on these projected differences, four combinations (dry and cold, dry and warm, wet and cold, and wet and warm) for each RCP were derived based on the 10^{th} and 90^{th} percentile values of the projected changes. Finally, the model run that was closest to the percentile values were selected for downscaling. The 10^{th} and 90^{th} percentile values were selected to include all four corners of the projected changes in temperature and precipitation and to avoid outlier GCMs. According to this method, four GCMs each were selected for both climate scenarios followed by downscaling of the model projections using the monthly delta change grids for the future (2021-2050) relative to a reference period (1961-1990) for each GCM (Immerzeel et al. 2013; Table 9). The delta change values in the grids reflect the change in temperature (K) and precipitation (%) over 60 years (Table 10).

TABLE 9. List of selected GCMs.

Description	RCP	dP (%)	dT (K)	Selected model
DRY, COLD	RCP 4.5	-1.8	1.4	GISS-E2_rcp45
DRY, WARM	RCP 4.5	-1.8	2.3	IPSL-CM5A_rcp45
WET, COLD	RCP 4.5	8.9	1.4	CCSM4_rcp45
WET, WARM	RCP 4.5	8.9	2.3	CanESM2_rcp45
DRY, COLD	RCP 8.5	-1.1	1.7	GFDL-ESM2G_rcp85
DRY, WARM	RCP 8.5	-1.1	2.7	IPSL-CM5A_rcp85
WET, COLD	RCP 8.5	12.1	1.7	CSIRO-Mk3_rcp85
WET, WARM	RCP 8.5	12.1	2.7	CanESM2_rcp85

Source: Lutz and Immerzeel 2013.

Notes: dP - Delta change value for precipitation; dT – Delta change value for temperature.

TABLE 10. Specification of delta change grids.

Character	Specification
Extent (WGS 1984)	Longitude: 66.00° to 99.00° E
	Latitude: 21.25° to 37.50° N
Spatial resolution	0.25° x 0.25°
ΔT units	Kelvin (K)
ΔP units	Percentage (%)
Format	American Standard Code for Information Interchange (ASCII) grid
Total number of grids	192

Delta Change Method

The monthly delta change grids for the future were then individually processed using GIS to obtain monthly delta change values for all the stations with precipitation and temperature data. There

are 92 precipitation stations, of which 53 have temperature stations. The delta change approach was used to generate daily future time series climate data (precipitation, maximum and minimum temperature) for the period 2021 to 2050 from the reference period (1998-2008); however, a period of 11 years (2040-2050) was used for climate change analysis. In order to generate future time series, we developed the R-model, which selects a random year from the reference period (1998-2008) and then applies the delta change formula (shown below) to generate future time series, with the assumption that the change from the period 1961-1990 until 2021-2050 is linear. More information on this method can be found in Wijngaard et al. (2017).

$$\boldsymbol{P_{i,j,k} = P_{i,j,baseyear} + P_{i,j,baseyear} * (\frac{dP_i}{60} * (k - baseyear + 1)/100}$$

$$\boldsymbol{T_{i,j,k} = T_{i,j,baseyear} + \frac{dT_i}{60} * (k - baseyear + 1)}$$

Where:
P = Precipitation (mm)
T = Temperature (maximum and minimum, °C)
i = day, $1 \leq i \leq 31$ for month *j*
j = month number, 1 (January) ≤ *j* ≤ 12 (December)
k = future year, $2021 \leq k \leq 2050$
baseline= 1998-2008
dP = delta change value for precipitation (%) for month *j*
dT = delta change value for temperature (K) for month

The SWAT model was then run with climate data (precipitation, maximum and minimum temperatures) generated by the delta change method for the projected period (2021-2050) for all eight GCMs for RCPs 4.5 and 8.5. The model output was then analyzed to assess the future change in hydrological components such as precipitation, actual ET, net water yield and discharge at Saptakoshi, which is the gauging point, with available data at the lowest reach of the basin.

RESULTS AND DISCUSSION

Water Balance

Temporal Distribution of Water Balance Components

After calibration and validation, the model was run from 1998 to 2008 with 2 years (1996-1997) as the warm-up period. The four hydrological components considered for the analysis were precipitation, actual evapotranspiration (ET), net water yield and the change in storage (Δ storage). Net water yield is the collective value of snowmelt, surface runoff, baseflow and lateral flow. It does not always follow the precipitation pattern, but is also affected by factors such as rainfall intensity, soil properties and land cover characteristics. The 'Δ storage' is a collective term including groundwater recharge, change in soil moisture storage in the vadose zone and model inaccuracies.

Annual average precipitation, actual ET and net water yield of the entire basin for the simulation period of 11 years were 1,720 mm, 520 mm and 1,124 mm, respectively. However, the temporal (Figure 13) and spatial variation (Figure 14) of these components within the basin is large. As can be seen from the monthly water balance in Figure 13, monsoon (June, July, August and September) is the main hydrological driver in the basin accounting for over 75% of precipitation and flows. As expected, actual ET and water yield are high in the monsoon and low in the dry period of the year. Large values of Δ storage during the monsoon can be attributed to high groundwater recharge, which is responsible for groundwater flow and ultimately baseflow during the dry period of the year. Similarly, a decreasing trend of Δ storage from the monsoon to the dry period is very prominent. July was identified as the wettest month with a maximum precipitation of 393 mm and December the driest with 9 mm. The annual average precipitation for the entire basin for the reference period is 1,720 mm, and the mean seasonal distribution is 49 mm, 241 mm, 1,345 mm and 84 mm for winter (December, January), pre-monsoon (February, March, April, May), monsoon (June, July, August) and post-monsoon (September, October, November) seasons, respectively. The average annual actual ET for the entire basin for the reference period is 550 mm and the mean seasonal distribution is 49 mm, 131 mm, 290 mm and 80 mm for winter, pre-monsoon, monsoon and post-monsoon seasons, respectively. The average annual ET is highest in the Indo-Gangetic Plains, owing to the greater area under cultivation and irrigation. Actual ET decreases from the Indo-Gangetic Plains to the transmountain region. The average annual net water yield for the reference period is 1,124 mm and mean seasonal distribution is 57 mm, 105 mm, 838 mm and 124 mm for winter, pre-monsoon, monsoon and post-monsoon seasons, respectively. Net water yield is highest in the mountains, followed by the hills, the Indo-Gangetic Plains and transmountain regions.

FIGURE 13. Mean monthly water balance (1998-2008).

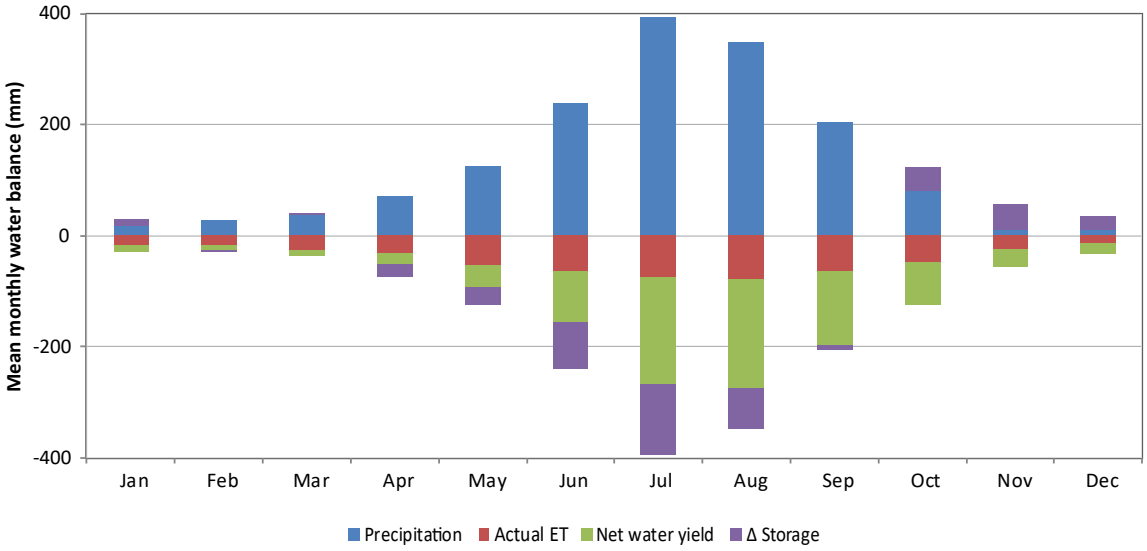

Spatial Distribution of Water Balance Components

Figures 14, 15 and 16 show the spatial distribution of annual average precipitation, actual ET and net water yield for the reference period (1998-2008). The precipitation and net water yield are lowest in the transmountain region and highest in the mountains followed by the hills in the Nepal part of the basin. In most of the upper sub-basins, water yield was greater than ET. An increasing trend of ET from the northern part to the southern part of the basin is prominent (Figure 15). As ET depends largely on precipitation, land cover and temperature, it was found to be high in forested areas in the hill regions of the basin and agricultural areas in the plains of Nepal and India. Maximum precipitation (5,135 mm) occurred in a sub-basin in the mountain region and minimum precipitation (604 mm) in the transmountain region in the Tibetan plateau. The maximum ET (1,052 mm) occurred in a sub-basin in the Indo-Gangetic Plains of India, while the minimum ET (52 mm) occurred in a sub-basin in the transmountain region of China. Similarly, the maximum water yield (4,408 mm) was recorded in a sub-basin in the mountain region of Nepal and the minimum water yield (259 mm) was recorded in a sub-basin of the transmountain region of China.

FIGURE 14. Spatial distribution of annual average precipitation.

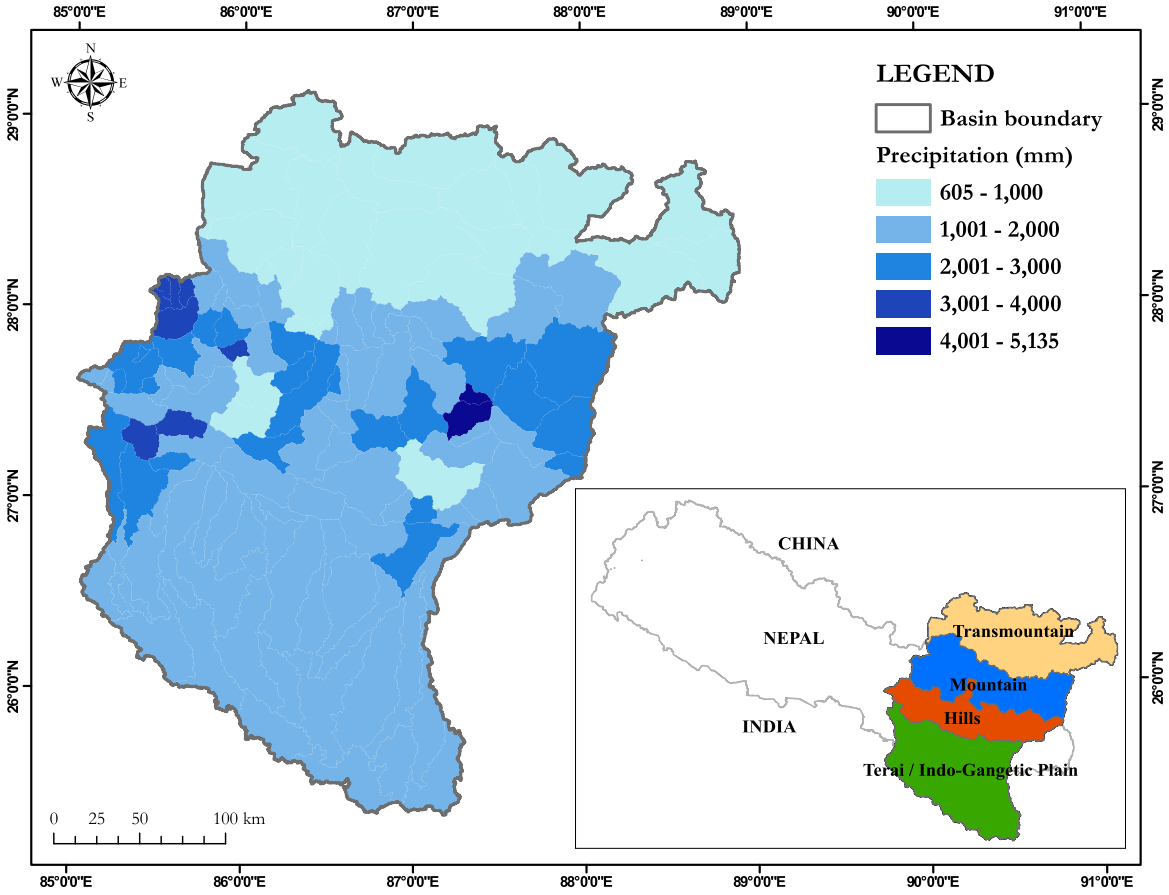

FIGURE 15. Spatial distribution of annual average actual evapotranspiration.

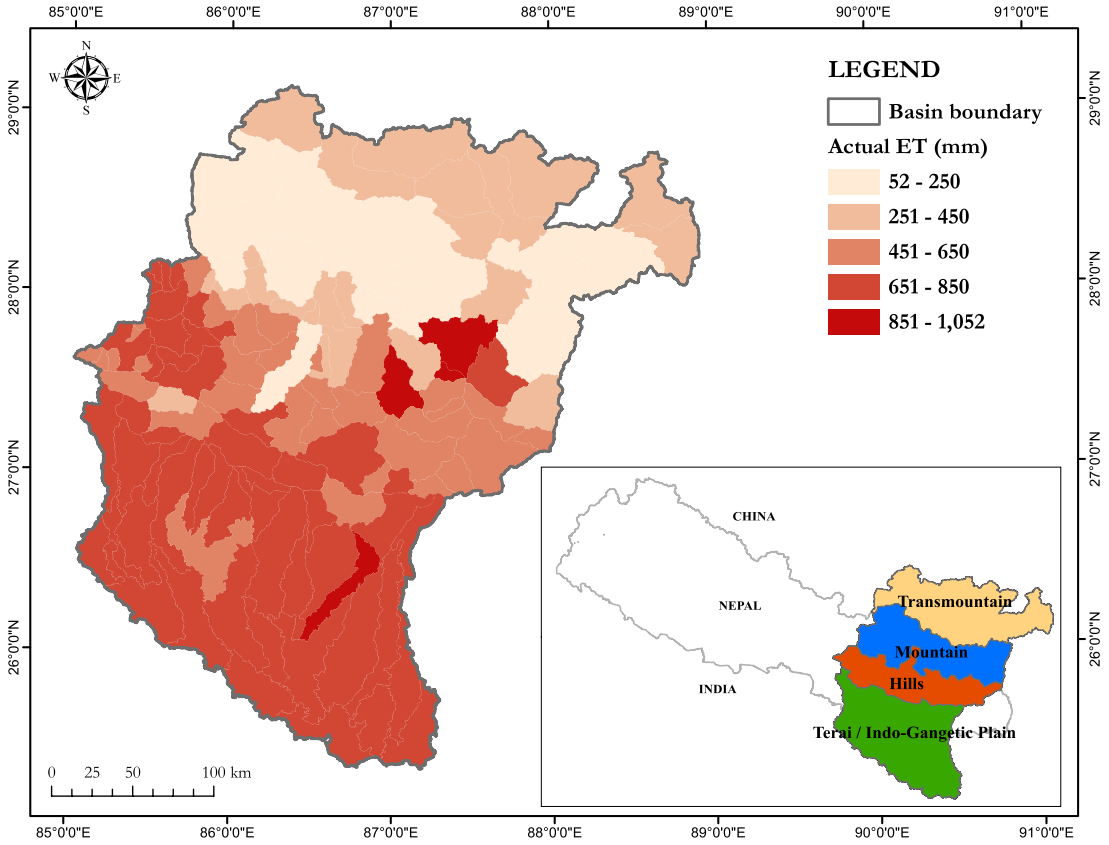

FIGURE 16. Spatial distribution of annual average net water yield.

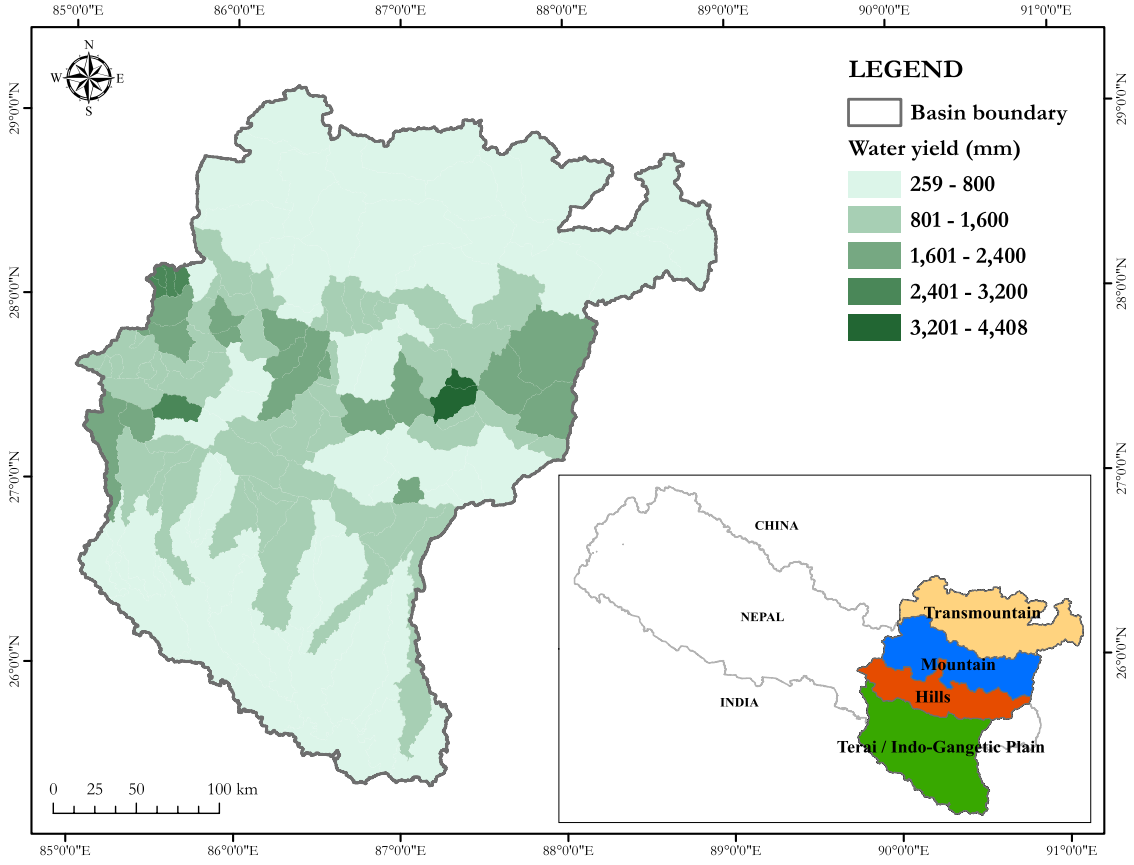

Ecological Region-wise Water Balance Calculations

Figure 17 shows the annual variation of precipitation, actual ET and net water yield in the different ecological regions within the Koshi Basin. The error bars show the maximum-minimum range for each parameter within the specified region. Maximum annual average precipitation (2,234 mm) was recorded in the mountain region (M) followed by the hills (H) and the Indo-Gangetic Plains (IGP), and the minimum (943 mm) was recorded in the transmountain region (TM). Annual average actual ET shows a different trend with a minimum (232 mm) in the TM, which increases as we move down the elevation of the basin with the maximum occurring in the IGP (763 mm). Annual net water yield follows a similar pattern to that of precipitation. Minimum net water yield occurs in the TM (585 mm) and the maximum occurs in the mountain region (1,675 mm). As seen in Figure 17, the maximum and minimum ranges for precipitation, actual ET and net water yield are highest in the mountain region and lowest in the transmountain region.

Figure 18 shows the seasonal variation of mean precipitation, mean actual ET and mean net water yield in the different ecological regions within the study basin. The error bars show the maximum-minimum range for each parameter within the specified region. Although the magnitudes vary, a very similar trend is observed in all the cases. Precipitation, actual ET and net water yield have the maximum values during the monsoon season followed by the pre-monsoon, post-monsoon and winter seasons. Mean precipitation is highest in the mountains, i.e., 61 mm during the winter, 278 mm in the pre-monsoon, 1,494 mm in the monsoon and 87 mm in the post-monsoon seasons. Variation in mean actual ET within the basin is low for a particular season. However, it is highest in the monsoon season with a maximum value of 1,277 mm in the mountains. Mean actual ET for the IGP is very similar for the pre- and post-monsoon seasons. As expected, the mean net water yield is also highest during the monsoon season followed by the pre-monsoon, post-monsoon and winter seasons. Areas with high actual ET have low water yields, e.g., the IGP. The highest net water yield is observed in the mountains during the monsoon season (1,063 mm).

The monsoon is clearly the main hydrological driver in the basin as precipitation, ET and water yield are the highest during this season. Storage and transferring water from the monsoon to the dry period is a good water management strategy. There is also a clear mismatch between areas where water availability is highest (mountains) to areas where water use is highest, i.e., in the Indo-Gangetic Plains. The water generated in the mountains in Nepal are, therefore, very important for maintaining the vast area of irrigated agriculture in the Indo-Gangetic Plains, termed the ‘bread basket’ in both Nepal and India.

Analysis of Extreme Flow Events

Indicators of Hydrologic Alteration (IHA) version 7.1 is a tool which can be easily used to summarize long periods of daily data. It was used to analyze the hydrologic characteristics of the Koshi River at Chatara using daily time series flow data from 1982 to 2006 (for further details, see Richter et al. 1996). Parametric statistics (mean/standard deviation) were used for the analysis. Flows exceeding 75% of daily flows for the period were classified as High Flows and those below 50% of daily flows for the period were classified as Low Flows. A Small Flood event was defined as an initial High Flow with a peak flow greater than a 2-year return interval event. Similarly, a Large Flood event was defined as an initial High Flow with a peak flow greater than a 10-year return interval event. An Extreme Low Flow was defined as an initial Low Flow below 10% of daily flows for the period.

Figure 19 shows the Flow Duration Curve (FDC) of Chatara for the reference period. Flows corresponding to 40%, 60% and 80% exceedance probabilities are 1,090 m^3/s, 543 m^3/s and 385 m^3/s, respectively.

FIGURE 17. Ecological region-wise variation of (a) annual precipitation, (b) actual ET, and (c) net water yield within the Koshi Basin.

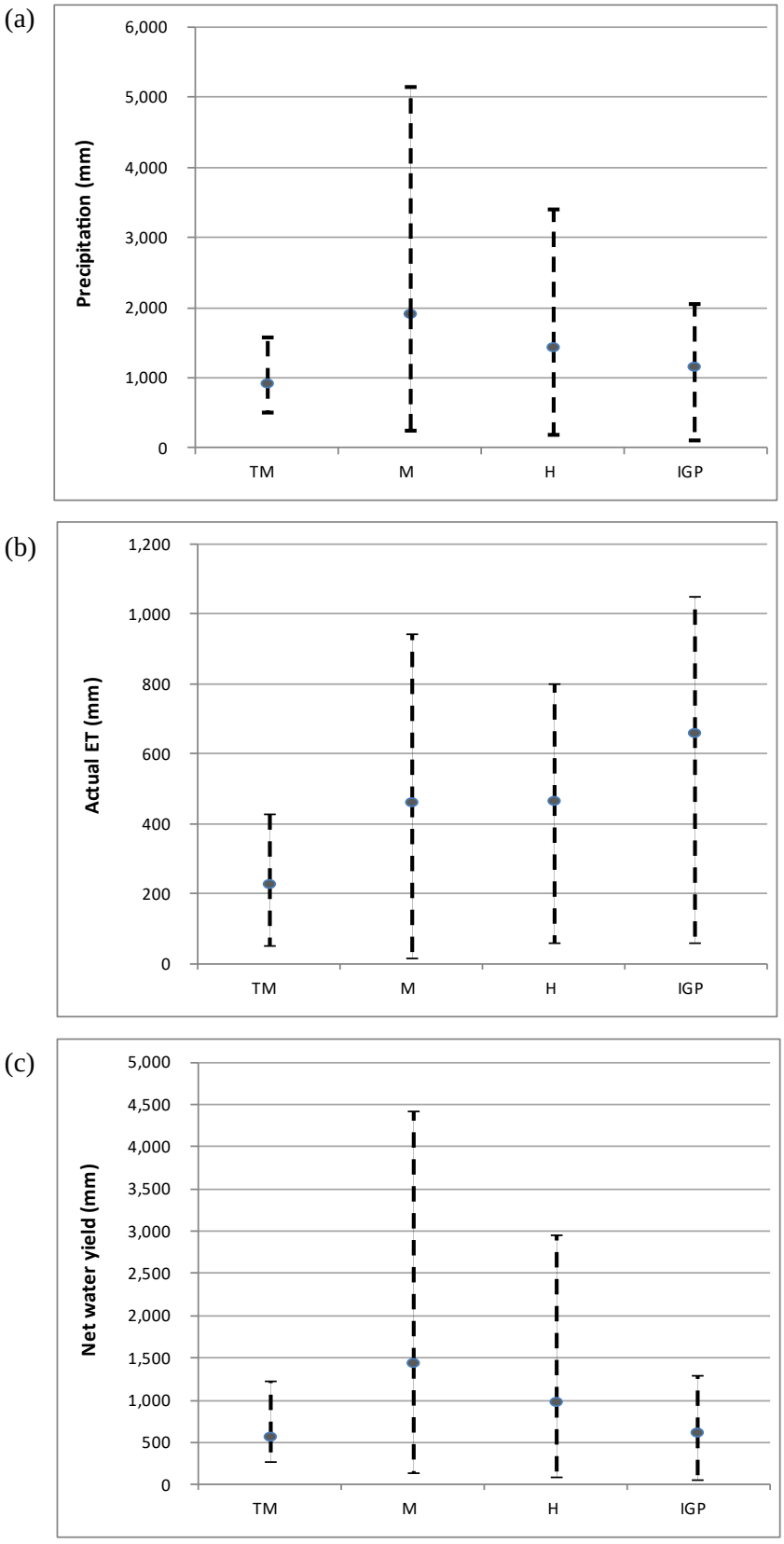

Notes: TM = Transmountain; M = Mountain; H = Hills; IGP = Indo-Gangetic Plains; error bars show the maximum-minimum range.

FIGURE 18. Ecological region-wise seasonal variation of (a) mean precipitation, (b) mean actual ET, and (c) mean net water yield within the Koshi Basin.

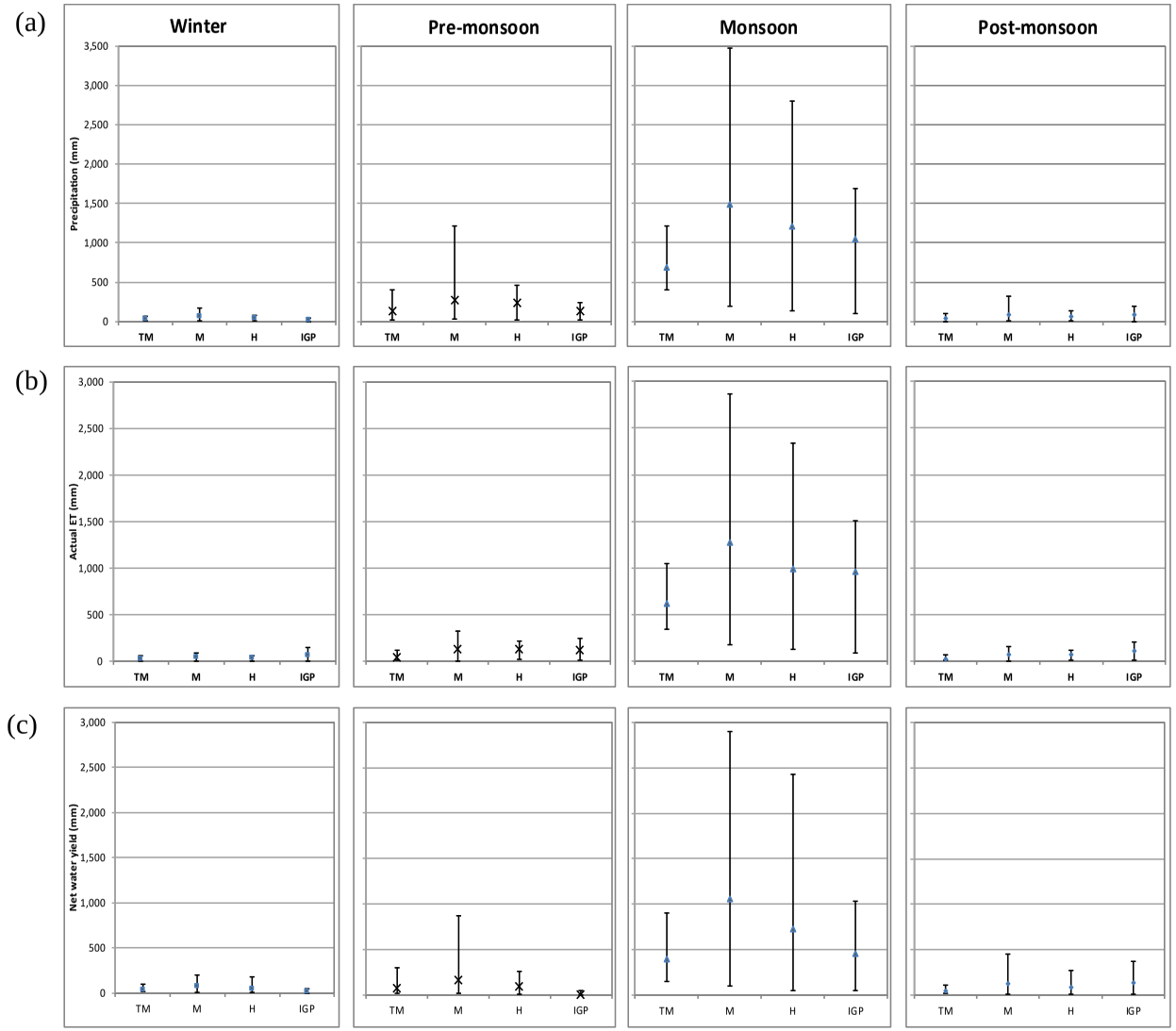

Notes: TM = Transmountain; M = Mountain; H = Hills; IGP = Indo-Gangetic Plains; error bars show the maximum-minimum range.

Figure 20 shows the environmental flow components at Chatara. It can be seen from the graph that small floods and high floods are very common, occurring almost every year during the monsoon. Two instances of large floods (in 1987 and 2003) can also be observed. Similarly, a few occurrences of extreme low flows can also be seen. Thus, it can be said that the Koshi River has a high degree of variability regarding its flow characteristics. The information on these extreme events could be very useful for water-induced disaster management in this region, and also for planning long-term hydraulic structures.

Results of the high-flow analysis are shown in Figure 21. It can be seen that peak flows within the range of 2,500-4,500 m^3/s are very common for the Koshi River at Chatara. Extreme flows (greater than 6,000 m^3/s) have also occurred in the past (2003-2004). It is also evident that high-flow pulses occur at least two to five times annually during the monsoon (June to August), and those pulses last for 2 to 20 days almost every year. An annual increasing trend is seen in the high-flow pulse frequency, and occurrences of high flows are shifting towards the latter part of the monsoon. As with large floods, small floods also occur during the monsoon.

Low-flow analysis is summarized in Figure 22. It is clear that, although the occurrence of low flows is relatively less frequent during the period of analysis, it extends to 70-100 days annually. Extreme low flows occur two to nine times annually with a duration of up to 25 days every year (Figure 22). These events are found to occur during the dry season. The frequent occurrences of both high- and low-flow events demonstrates the vulnerability of the region to both floods and droughts, resulting in a very risk-prone livelihood system.

Results from RCPs 4.5 and 8.5 Future Projections

Figures 23, 24 and 25 show sub-basin-wise average percentage changes in precipitation, actual ET and net water yield, respectively, for four GCMs each of RCPs 4.5 and 8.5. Precipitation and net water yield show increases in most parts of the basin except for the sub-basins within the transmountain region, which shows a decrease. Similarly, Actual ET is seen to increase over the entire basin except for a few sub-basins, especially in the transmountain region. The RCP 8.5 projections show a similar spatial pattern to RCP 4.5. Actual ET is projected to increase across most of the basin, and precipitation and water yield will increase except in a few sub-basins, which are mostly in the transmountain region.

Figure 26 shows the monthly minimum, maximum and average discharges for the reference period (1998-2008) and projected period (2040-2050) for ensembles of RCP 4.5 for Chatara gauging station (Figure 4). The data range for the reference period is represented by the error bars and the range for all the CC projections are within the orange area in the figure. As variability is high in the basin, it is useful to compare future changes in the data range in addition to the average changes. If, for example, the future range is similar to the past range then adaptation strategies might already exist, which then decreases vulnerability. However, if the future range is outside of the past range then the impact of CC will be more severe. For RCP 4.5, the lower range for the projected average monthly discharge is within the range of the discharge in the reference period for all the months. Therefore, the future low flows are within the past data range. However, the range for the projected high flows is outside the past range in all the months except January and September. This suggests that the peak flows will increase in the future, also increasing the risk of floods. The average seasonal discharge from the different projections shows an increase for all seasons, i.e., 2 to 12% in the winter, 5 to 13% in the pre-monsoon, -2% to 11% in the monsoon and 5 to 16% in the post-monsoon seasons.

FIGURE 19. Flow duration curve (FDC) in log scale of Chatara.

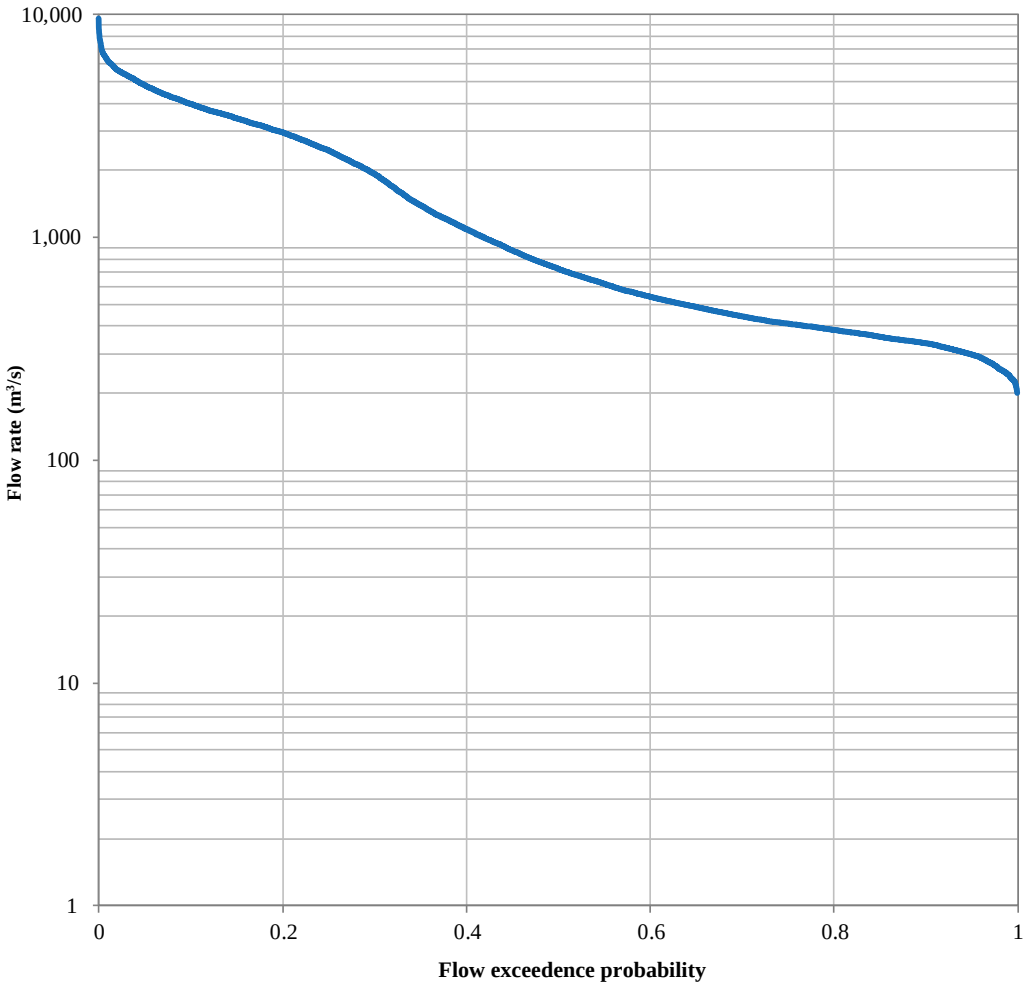

Figure 27 shows the monthly minimum, maximum and average discharges for the reference period (1998-2008) and projected period (2040-2050) for ensembles of RCP 8.5 for Chatara gauging station. Similar to Figure 26, the error bars and orange area show the minimum and maximum range of the reference period and projected period, respectively. For RCP 8.5, the projected average monthly discharges during low flows are within the data range for the reference period. However, the projected monthly average discharge from May until November is higher than the past range. The average seasonal discharge from the different projections also shows an increase for all seasons under RCP 8.5, i.e., 8 to 14% in the winter, -8 to 25% in the pre-monsoon, 9 to 18% in the monsoon and 3 to 20% in the post-monsoon seasons.

Therefore, both Figures 26 and 27 suggest that the future changes during the dry season (November-May) are within the past ranges. However, the future monsoon flows will be higher than the past as demonstrated by higher averages as well as maximum flows.

Results show that the seasonal variation in contribution to annual flow volume at the outlet of the Koshi Basin for the reference and projected periods remained very similar. For the reference period, 72% of the total annual flow occurred during the monsoon, 6% in the winter, 12% in the pre-monsoon and 10% in the post-monsoon seasons. The projected variation in seasonal contribution to annual flow only showed a 1% change in the monsoon season and a maximum of a 2% change in the pre-monsoon season. The percentage contributed was the same for both the post-monsoon and winter seasons.

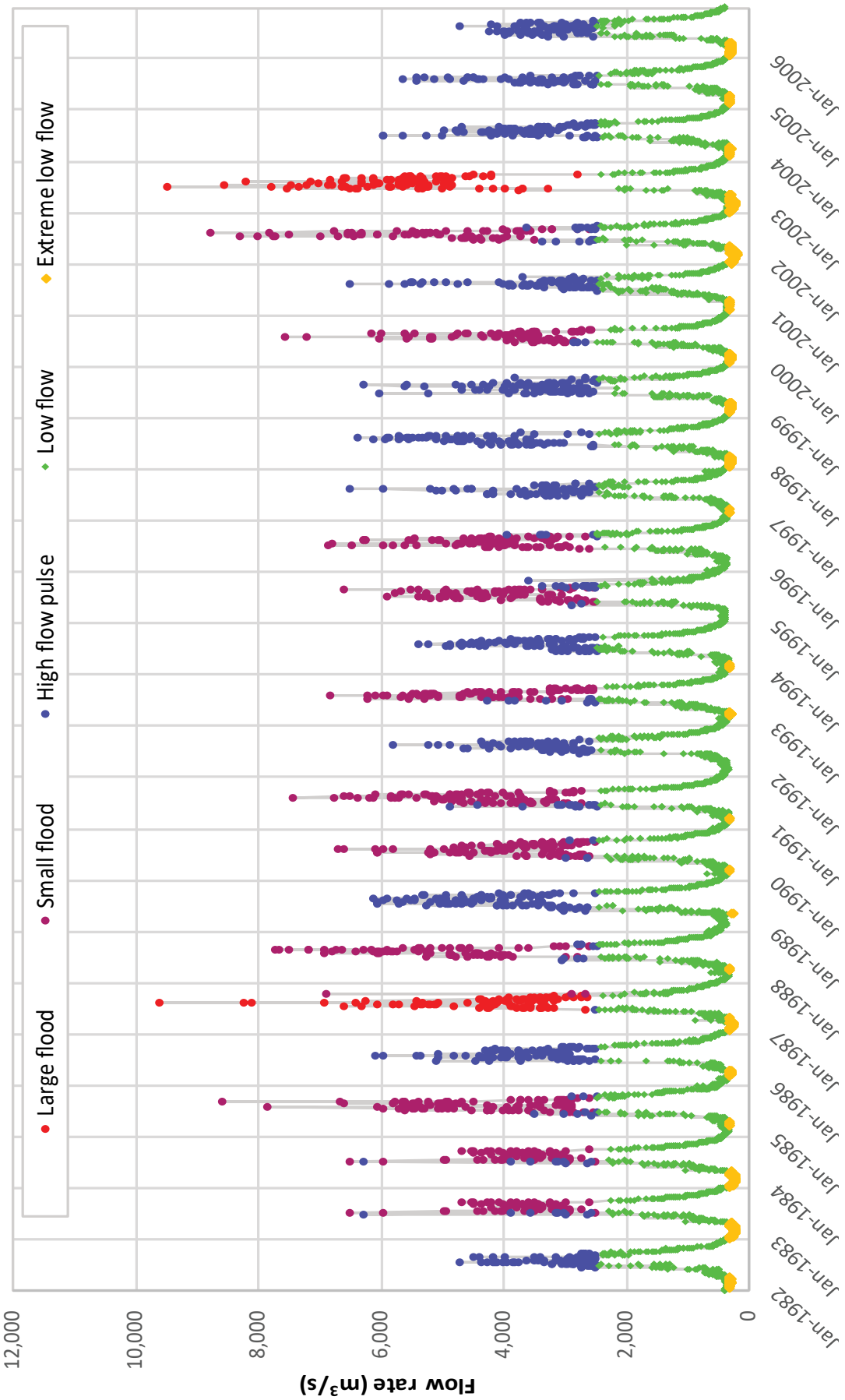

FIGURE 20. Environmental flow components: Extreme low flows, low flows, high flow pulses, small floods and large floods at Chatara.

FIGURE 21. Results of the high-flow analysis: (a) peak, (b) frequency, (c) timing, and (d) duration.

(a)

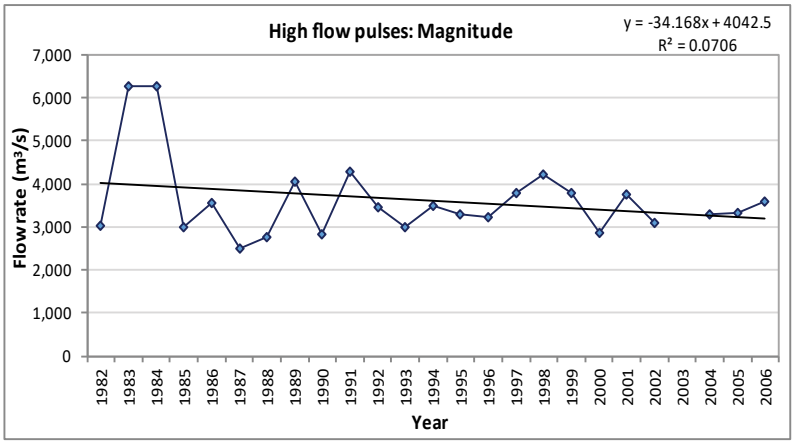

(b)

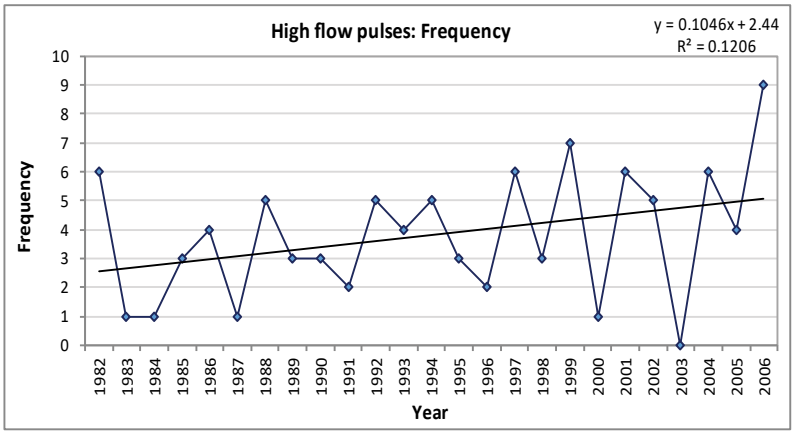

(c)

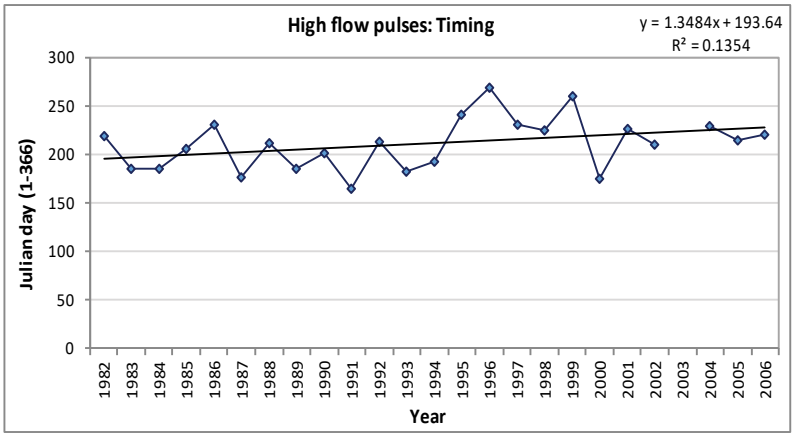

(d)

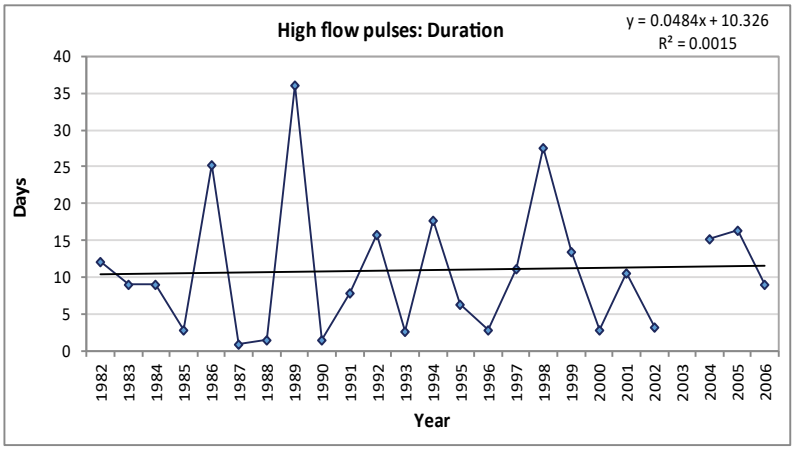

FIGURE 22. Results of extreme low-flow analysis: (a) low flows, (b) frequency, (c) timing, and (d) duration.

(a)

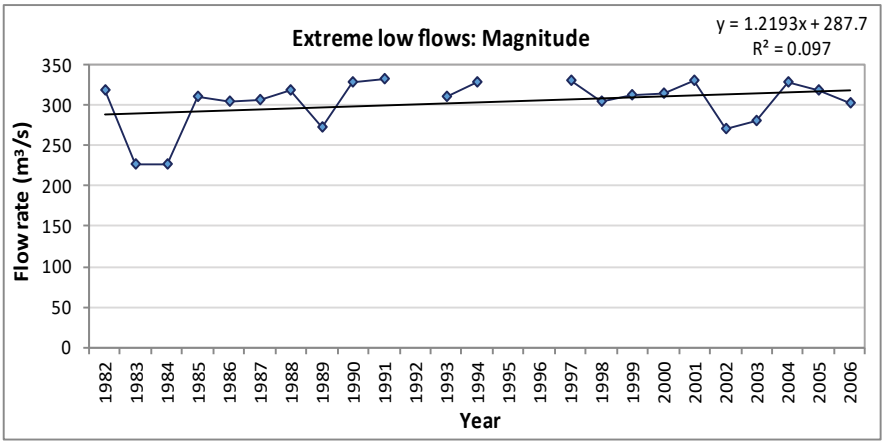

(b)

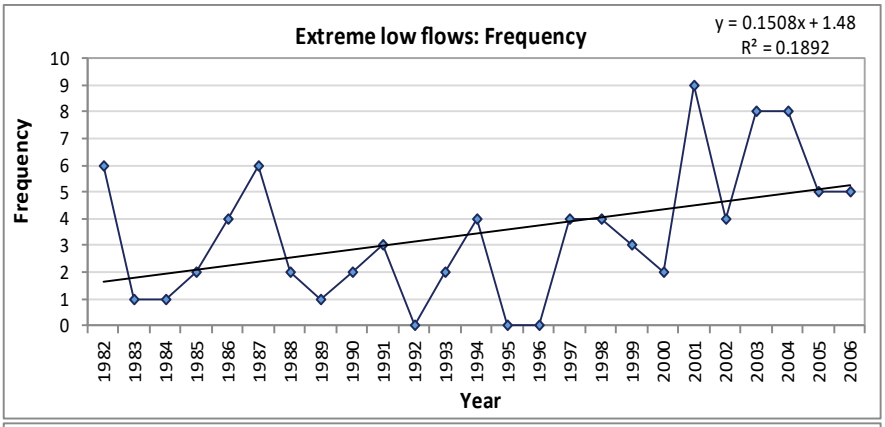

(c)

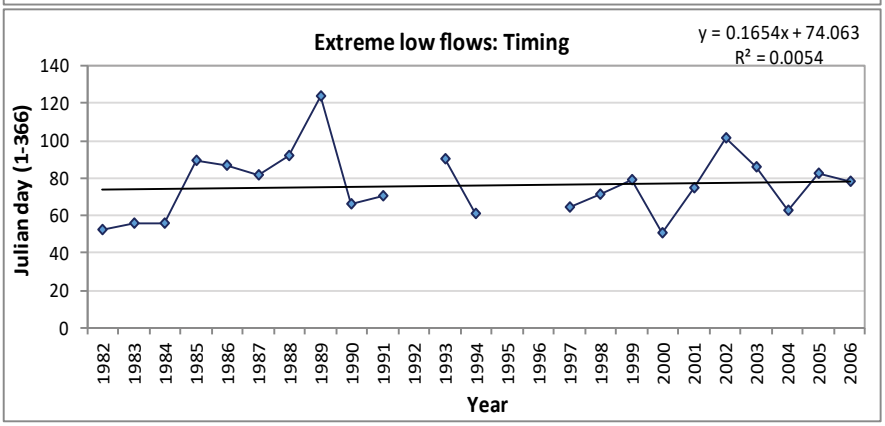

(d)

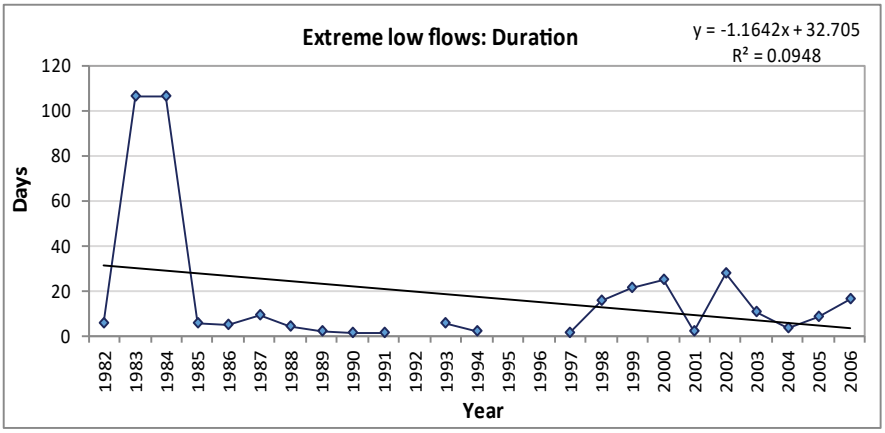

FIGURE 23. Future projection (2040-2050) of precipitation for (a) RCP 4.5, and (b) RCP 8.5.

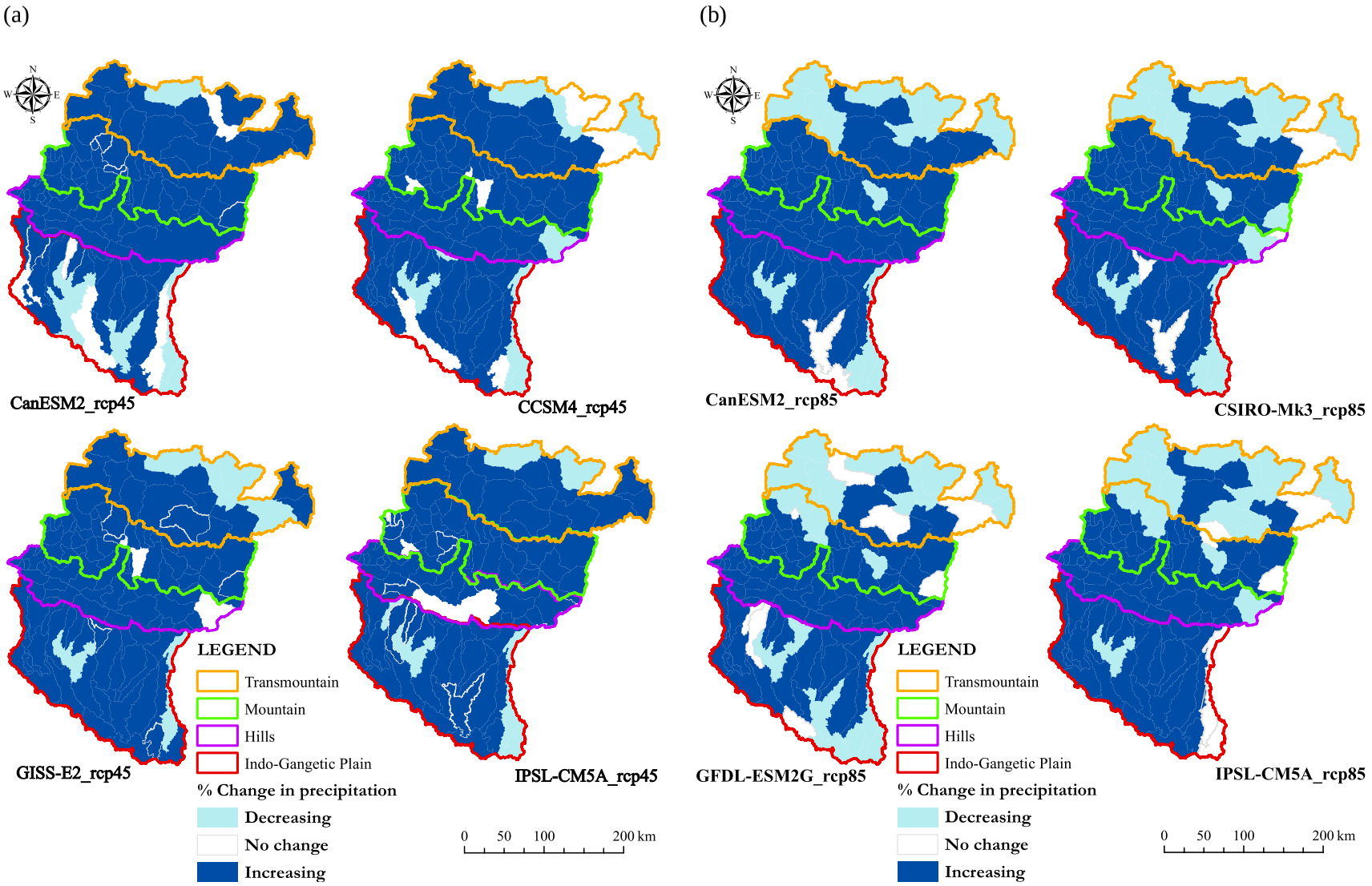

Note: Refer to Table 9 for details on the GCMs for each scenario.

FIGURE 24. Future projection (2040-2050) of actual ET for (a) RCP 4.5, and (b) RCP 8.5.

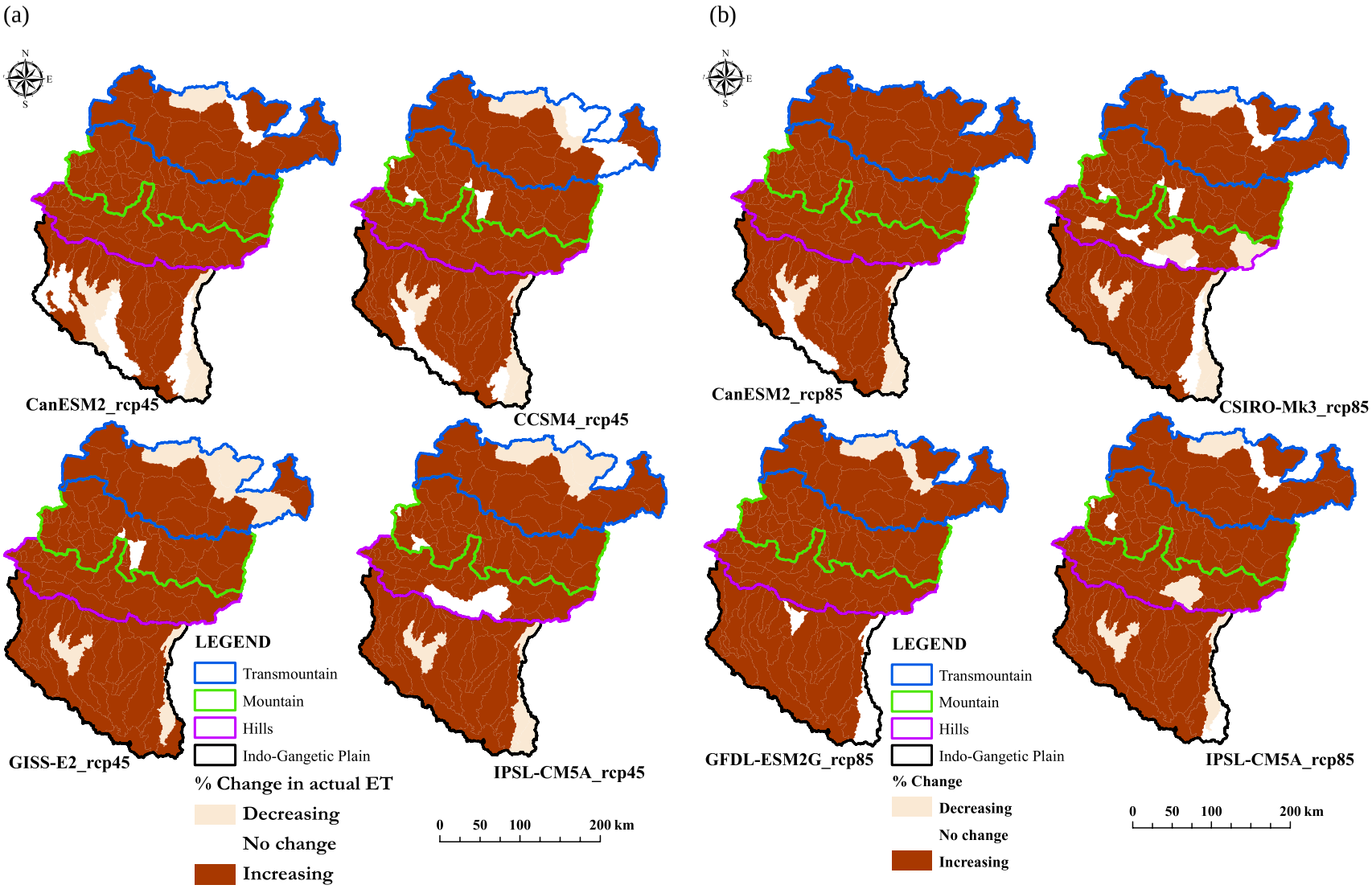

Note: Refer to Table 9 for details on the GCMs for each scenario.

FIGURE 25. Future projection (2040-2050) of net water yield for (a) RCP 4.5, and (b) RCP 8.5.

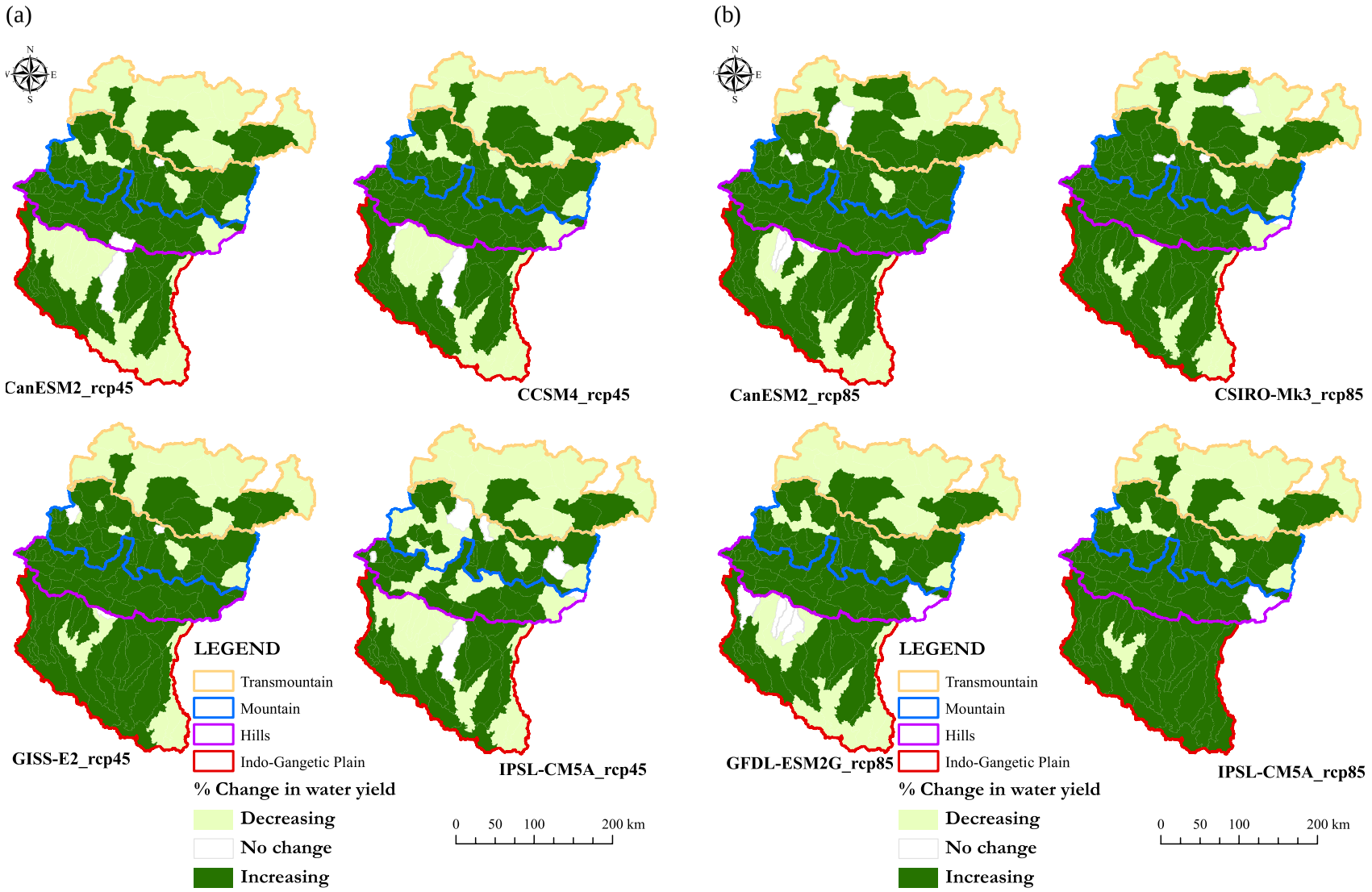

Note: Refer to Table 9 for details on the GCMs for each scenario.

FIGURE 26. Average annual hydrograph for the reference (1998-2008) and future (2040-2050) periods for ensembles of RCP 4.5.

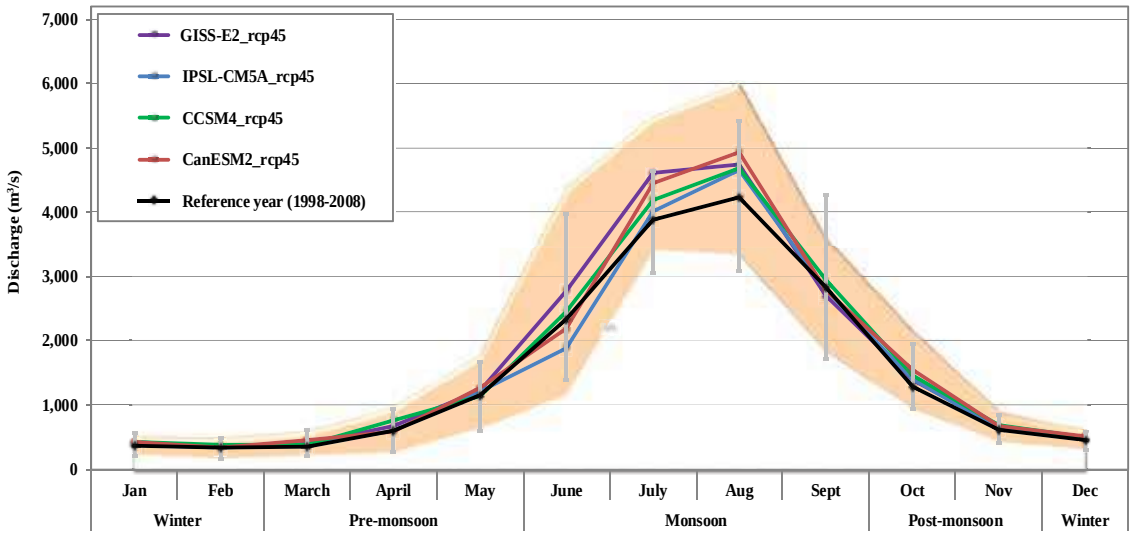

FIGURE 27. Average annual hydrograph for the reference (1998-2008) and future (2040-2050) periods for ensembles of RCP 8.5.

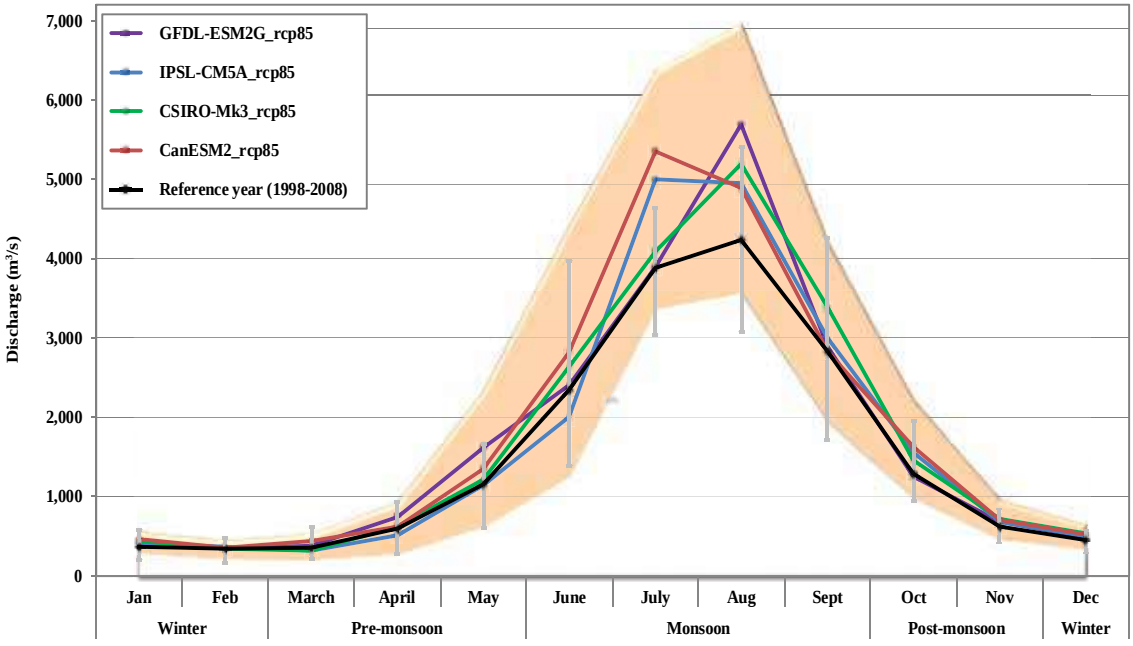

CONCLUSIONS

This study developed a SWAT for the Koshi Basin using in situ and remotely sensed data and evaluated CC impacts under eight future scenarios. Analysis of past (1998 to 2008) water balance indicates that approximately 65% of average annual precipitation (1,720 mm) is converted to flows (1,124 mm). Therefore, water availability in the Koshi Basin is very high. Both net water yield and precipitation are highest in the mountains, followed by hills, the Indo-Gangetic Plains and transmountain region. The average annual actual ET is highest in the Indo-Gangetic Plains, owing to the greater area under cultivation. Actual ET, a proxy for water use by plants, is high in areas which are forested and used for agriculture, especially irrigated agriculture. The fact that there is a mismatch between areas where water availability is highest (mountains) and areas where water use is highest (Indo-Gangetic Plains) has been creating tension in basin water planning and management. This issue is exacerbated due to all of the mountain region with high water availability being in Nepal and most of the plains area with high water use due to irrigated agriculture in India. Most of the transboundary issues stem from this mismatch in water availability and use between the sub-basins in Nepal and India. As most of the water from the mountain and hill regions eventually flow down to the plains, the mountain and hill regions in Nepal are very important for maintaining agriculture in the plains in both Nepal and India.

The high- and low-flow analysis shows high-flow (exceeding 75% of mean daily flows) pulses occur two to five times annually and last for 2 to 20 days during the monsoon season. Extreme low flows occur two to nine times annually and last up to 25 days during dry season, indicating high temporal variation of flows in the Koshi Basin. Therefore, there is a high degree of variability in flow characteristics reflecting the “too much and too little water” problems that are often discussed for the region. The monsoon accounts for over 75% of precipitation and flows. Therefore, the monsoon is still the main hydrological driver. Winter precipitation is, however, still important to replenish the soil moisture needed for winter crops.

Results from RCPs 4.5 and 8.5 future projections indicate an increase in actual ET in most of the basin, and also an increase in precipitation and net water yield in a larger part of the basin, except for a few sub-basins which are mostly in the transmountain region. Comparison of flow ranges between the past and projected data indicate that the future changes during the dry season (November-May) are within the past ranges. However, the future monsoon flows will be higher than the past as demonstrated by higher averages as well as maximum flows. Therefore, flooding occurrences are expected to increase with CC.

Countries comprising the Koshi Basin (Nepal, India and China) routinely feature on lists of the most climate-vulnerable nations in the world, which is due to both drought and flood risks. Already, the Koshi is termed the “sorrow of Bihar” as frequent floods kill hundreds of people and affect thousands of hectares of agricultural land on an annual basis.

Results from this study show a high likelihood of stronger monsoons, which will increase impacts and risks for monsoon-related disasters, such as landslides and floods, in the future. Therefore, disaster risk reduction and management, especially related to floods, should be a priority of the governments of Nepal, India and China.

Due to high water availability, the Koshi Basin is seen as having high potential for hydropower and irrigation development. Most planning in the basin is still done at individual project level without considering the impact at the basin scale. Hydropower and irrigation projects are also being designed without considering the impacts of future CC. This study, therefore, also hopes to contribute to the knowledge and information base to promote basin-level planning and safeguarding against future CC impacts in the Koshi Basin.

REFERENCES

Agarwal, A.; Babel, M.S.; Maskey, S. 2014. Analysis of future precipitation in the Koshi river basin, Nepal. *Journal of Hydrology* 513: 422-434. https://doi.org/10.1016/j.jhydrol.2014.03.047

Agarwal, A.; Babel, M.S.; Maskey, S.; Shrestha, S.; Kawasaki, A.; Tripathi, N.K. 2016. Analysis of temperature projections in the Koshi River Basin, Nepal. *International Journal of Climatology* 36(1): 266-279. https://doi.org/10.1002/joc.4342

Arnold, J.G.; Srinivasan, P.; Muttiah, R.S.; Williams, J.R. 1998. Large area hydrologic modelling and assessment. Part I: Model development. *Journal of the American Water Resources Association* 34(1): 73-89. https://doi.org/10.1111/j.1752-1688.1998.tb05961.x

Arnold, J.G.; Kiniry, J.R.; Srinivasan, R.; Williams, J.R.; Haney, E.B.; Neitsch, S.L. 2011. *Soil and Water Assessment Tool: Input/output file documentation, version 2009*. Texas Water Resources Institute Technical Report No. 365. Texas, USA: Texas Water Resources Institute.

Arnold, J.G.; Moriasi, D.N.; Gassman, P.W.; Abbaspour, K.C.; White, M.J.; Srinivasan, R.; Santhi, C.; Harmel, D.; van Griensven, A.; Van Liew, M.W.; Kannan, N.; Jha, M.K. 2012. SWAT: Model use, calibration, and validation. *Transactions of the American Society of Agricultural and Biological Engineers (ASABE)* 55(4): 1491-1508. https://digitalcommons.unl.edu/cgi/viewcontent.cgi?article=1408&context=biosysengfacpub

Bharati, L.; Gurung, P.; Jayakody, P.; Smakhtin, V.; Bhattarai, U. 2014. The projected impact of climate change on water availability and development in the Koshi Basin, Nepal. *Mountain Research and Development* 34(2): 118-131. https://doi.org/10.1659/MRD-JOURNAL-D-13-00096.1

Bharati, L.; Gurung, P.; Maharjan, L.; Bhattarai, U. 2016 Past and future variability in the hydrological regime of the Koshi Basin, Nepal. *Hydrological Sciences Journal* 61(1): 79-93. https://doi.org/10.1080/02626667.2014.952639

Bhatt, D.; Maskey, S.; Babel, M.S.; Uhlenbrook, S.; Prasad, K.C. 2014. Climate trends and impacts on crop production in the Koshi River basin of Nepal. *Regional Environmental Change* 14(4): 1291-1301. https://doi.org/10.1007/s10113-013-0576-6

Devkota, L.P.; Gyawali, D.R. 2015. Impacts of climate change on hydrological regime and water resources management of the Koshi River Basin, Nepal. *Journal of Hydrology: Regional Studies* 4(B): 502-515.

FAO (Food and Agriculture Organization of the United Nations); ISRIC (World Soil Information). 1990. *Guidelines for profile description*. 3rd Edition. Rome: Food and Agriculture Organization of the United Nations (FAO).

Gosain, A.K.; Rao, S.; Basuray, D. 2006. Climate change impact assessment on hydrology of Indian river basins. C*urrent Science* 90(3): 346-353.

Immerzeel, W.W.; Pellicciotti, F.; Bierkens, M.F.P. 2013. Rising river flows throughout the twenty-first century in two Himalayan glacierized watersheds. *Nature Geoscience* 6: 742-745. https://doi.org/10.1038/ngeo1896

IPCC (Intergovernmental Panel on Climate Change). 2014. Summary for policymakers. In: *Climate change 2014: Impacts, adaptation, and vulnerability. Part A: Global and sectoral aspects. Contribution of Working Group II to the Fifth Assessment Report of the Intergovernmental Panel on Climate Change*, (eds.) Field, C.B.; Barros, V.R.; Dokken, D.J.; Mach, K.J.; Mastrandrea, M.D.; Bilir, T.E.; Chatterjee, M.; Ebi, K.L.; Estrada, Y.O.; Genova, R.C.; Girma, B.; Kissel, E.S.; Levy, A.N.; MacCracken, S.; Mastrandrea, P.R.; White, L.L. Cambridge, United Kingdom and New York, NY, USA: Cambridge University Press. Pp. 1-32. Available at http://www.ipcc.ch/report/ar5/ (accessed on January 30, 2019).

Khadka, D.; Babel, M.S.; Shrestha, S.; Tripathi, N.K. 2014. Climate change impact on glacier and snow melt and runoff in Tamakoshi basin in the Hindu Kush Himalayan (HKH) region. *Journal of Hydrology* 511: 49-60. https://doi.org/10.1016/j.jhydrol.2014.01.005

Lacombe, G.; McCartney, M. 2014. Uncovering consistencies in Indian rainfall trends observed over the last half century. *Climatic Change* 123(2): 287-299. https://doi.org/10.1007/s10584-013-1036-5

Lutz, A.F.; Immerzeel, W.W. 2013. *Water availability analysis for the upper Indus, Ganges, Brahmaputra, Salween and Mekong river basins*. Final Report to the International Centre for Integrated Mountain Development (ICIMOD). FutureWater Report 127. Wageningen, The Netherlands: FutureWater.

Lutz, A.F.; Immerzeel, W.W.; Shrestha, A.B.; Bierkens, M.F.P. 2014. Consistent increase in High Asia's runoff due to increasing glacier melt and precipitation. *Nature Climate Change* 4: 587-592. https://doi.org/10.1038/nclimate2237

Miller, J.D.; Immerzeel, W.W.; Rees, G. 2012. Climate change impacts on glacier hydrology and river discharge in the Hindu Kush-Himalayas: A synthesis of the scientific basis. *Mountain Research and Development* 32(4): 461-468. https://doi.org/10.1659/MRD-JOURNAL-D-12-00027.1

Moriasi, D.N.; Arnold, J.G.; Van Liew, M.W.; Bingner, R.L.; Harmel, R.D.; Veith, T.L. 2007. Model evaluation guidelines for systematic quantification of accuracy in watershed simulations. *Transactions of the American Society of Agricultural and Biological Engineers (ASABE)* 50(3): 885-900.

Nepal, S. 2016. Impacts of climate change on the hydrological regime of the Koshi river basin in the Himalayan region. *Journal of Hydro-environment Research* 10: 76-89. https://doi.org/10.1016/j.jher.2015.12.001

Perrin, C.; Michel, C.; Andréassian, V. 2003. Improvement of a parsimonious model for streamflow simulation. *Journal of Hydrology* 279(1-4): 275-289. https://doi.org/10.1016/S0022-1694(03)00225-7

Qi, M.Q.; Redmann, R.E. 1993. Seed germination and seedling survival of C3 and C4 grasses under water stress. *Journal of Arid Environments* 24(3): 277-285. https://doi.org/10.1006/jare.1993.1024

Rahman, K.; Maringanti, C.; Beniston, M.; Widmer, F.; Abbaspour, K.; Lehmann, A. 2013 Streamflow modeling in a highly managed mountainous glacier watershed using SWAT: the Upper Rhone River watershed case in Switzerland. *Water Resources Management* 27(2): 323-339. https://doi.org/10.1007/s11269-012-0188-9

Richter, B.D.; Baumgartner, J.V.; Powell, J.; Braun, D.P. 1996. A method for assessing hydrologic alteration within ecosystems. *Conservation Biology* 10(4): 1163-1174. https://doi.org/10.1046/j.1523-1739.1996.10041163.x

Santhi, C.; Arnold, J.G.; Williams, J.R.; Dugas, W.A.; Srinivasan, R.; Hauck, L.M. 2001. Validation of the SWAT model on a large river basin with point and nonpoint sources. *Journal of the American Water Resources Association* 37(5): 1169-1188. https://doi.org/10.1111/j.1752-1688.2001.tb03630.x

Sharma, K.P.; Moore, B.; Vorosmarty, C.J. 2000. Anthropogenic, climatic, and hydrologic trends in the Koshi basin, Himalaya. *Climatic Change* 47(1-2): 141-165. https://doi.org/10.1023/A:1005696808953

Shrestha, S.; Gyawali, B.; Bhattarai, U. 2013. Impacts of climate change on irrigation water requirements for rice-wheat cultivation in Bagmati River Basin, Nepal. *Journal of Water and Climate Change* 4(4): 422-439. https://doi.org/10.2166/wcc.2013.050

Srinivasan, R.; Ramanarayanan, T.S.; Arnold, J.G.; Bednarz, S.T. 1998. Large area hydrologic modeling and assessment. Part II: Model application. *Journal of the American Water Resources Association* 34(1): 91-101. https://doi.org/10.1111/j.1752-1688.1998.tb05962.x

van Vuuren, D.P.; Edmonds, J.; Kainuma, M.; Riahi, K.; Thomson, A.; Hibbard, K.; Hurtt, G.C.; Kram, T.; Krey, V.; Lamarque, J-F.; Masui, T.; Meinshausen, M.; Nakicenovic, N.; Smith, S.J.; Rose, S.K. 2011. The representative concentration pathways: An overview. *Climatic Change* 109: 5-31. https://doi.org/10.1007/s10584-011-0148-z

Vrugt, J.A.; ter Braak, C.J.F.; Gupta, H.V.; Robinson, B.A. 2009. Equifinality of formal (DREAM) and informal (GLUE) Bayesian approaches in hydrologic modeling? *Stochastic Environmental Research and Risk Assessment* 23(7): 1011-1026. https://doi.org/10.1007/s00477-008-0274-y

Wijngaard, R.R.; Lutz, A.F.; Nepal, S.; Khanal, S.; Pradhananga, S.; Shrestha, A.B.; Immerzeel, W.W. 2017. Future changes in hydro-climatic extremes in the Upper Indus, Ganges, and Brahmaputra River basins. *PLoS ONE* 12(12): e0190224. https://doi.org/10.1371/journal.pone.0190224

IWMI Working Papers

187 *From the Mountains to the Plains: Impact of Climate Change on Water Resources in the Koshi River Basin.* Luna Bharati, Utsav Bhattarai, Ambika Khadka, Pabitra Gurung, Luis E. Neumann, David J. Penton, Sanita Dhaubanjar and Santosh Nepal. 2019.

186 *Unpacking the Water-Energy-Environment-Food Nexus: Working Across Systems*. Aditya Sood, Alan Nicol and Indika Arulingam. 2019.

185 *Improving the Availability and Effectiveness of Rural and "Micro" Finance for Small-scale Irrigation in Sub-Saharan Africa: A Review of Lessons Learned.* Douglas J. Merrey and Nicole Lefore. 2018.

184 *Gender Dimensions of Community-based Groundwater Governance in Ethiopia: Using Citizen Science as an Entry Point*. Likimyelesh Nigussie, Jennie Barron, Alemseged Tamiru Haile, Nicole Lefore and John Gowing. 2018.

183 *Community-managed Groundwater Irrigation on the Vientiane Plain of Lao PDR: Planning, Implementation and Findings from a Pilot Trial.* Corentin Clément, Jordan Vinckevleugel, Paul Pavelic, Kong Xiong, Lengya Valee, Touleelor Sotoukee, Binaya Raj Shivakoti and Khammai Vongsathiane. 2018.

182 *Highlights of Soil and Water Conservation Investments in Four Regions of Ethiopia*. Zenebe Adimassu, Simon Langan and Jennie Barron. 2018.

181 *Investigation of the Modalities for an Innovative Financing Mechanism for Participatory Natural Resource Management in the Bale Eco-region, Ethiopia.* Fitsum Hagos, Daniel van Rooijen, Amare Haileslassie, Habtamu Yehualashet and Husien Indries. 2018.

180 *Water User Associations: A Review of Approaches and Alternative Management Options for Sub-Saharan Africa.* Eefje Aarnoudse, Alvar Closas and Nicole Lefore. 2018.

179 *Dependence of Riparian Communities on Ecosystem Services in Northern Ghana.* Marloes Mul, Laetitia Pettinotti, Naana Adwoa Amonoo, Emmanuel Bekoe-Obeng and Emmanuel Obuobie. 2017.

178 *Understanding the Hydrological Impacts of Climate Change in the Tana River Basin, Kenya.* Aditya Sood, Lal Muthuwatta, Nishchitha Sandeepana Silva and Matthew McCartney. 2017.

Postal Address
P O Box 2075
Colombo
Sri Lanka

Location
127 Sunil Mawatha
Pelawatta
Battaramulla
Sri Lanka

Telephone
+94-11-2880000

Fax
+94-11-2786854

E-mail
iwmi@cgiar.org

Website
www.iwmi.org

IWMI is a CGIAR Research Center and leads the: CGIAR RESEARCH PROGRAM ON Water, Land and Ecosystems

ISSN: 2012-5763
e-ISSN: 2478-1134
ISBN: 978-92-9090-885-2